LAWRENCE
LIVERMORE
NATIONAL
LABORATORY

UCRL-JRNL-215684

A High-Order Accurate Parallel Solver for Maxwell's Equations on Overlapping Grids

William D. Henshaw

September 27, 2005

SIAM Journal of Scientific Computing

A HIGH-ORDER ACCURATE PARALLEL SOLVER FOR MAXWELL'S EQUATIONS ON OVERLAPPING GRIDS

WILLIAM D. HENSHAW*

Abstract. A scheme for the solution of the time dependent Maxwell's equations on composite overlapping grids is described. The method uses high-order accurate approximations in space and time for Maxwell's equations written as a second-order vector wave equation. High-order accurate symmetric difference approximations to the generalized Laplace operator are constructed for curvilinear component grids. The modified equation approach is used to develop high-order accurate approximations that only use three time levels and have the same time-stepping restriction as the second-order scheme. Discrete boundary conditions for perfect electrical conductors and for material interfaces are developed and analyzed. The implementation is optimised for component grids that are Cartesian, resulting in a fast and efficient method. The solver runs on parallel machines with each component grid distributed across one or more processors. Numerical results in two- and three-dimensions are presented for the the fourth-order accurate version of the method. These results demonstrate the accuracy and efficiency of the approach.

Key words. Maxwell's equations, overlapping grids, high-order accurate, symmetric finite difference

1. Introduction. A numerical scheme is described for the fast and accurate solution of the time dependent Maxwell's equations in complex geometry. Maxwell's equations are solved as a second-order vector wave-equation rather than the more common approach of treating the equations as a first-order system. The governing equations are discretized to high-order accuracy in space and time on domains that are represented with composite overlapping grids. High-order accurate symmetric finite difference discretizations of the generalized Laplace operator are devised, for use on curvilinear grids. High-order accurate centered approximations for boundary conditions are developed and analyzed. The three-level time stepping scheme is based on the modified equation approach and achieves high-order accuracy by including approximations to higher spatial derivatives. The time step restriction, as dictated by stability, is the same as that used with the second-order version of the method. The interface between materials with different electric and magnetic properties is treated using component grids that align with the interface. High-order accurate centered approximations to the interface jump conditions are developed that maintain the full accuracy of the scheme at the interface. The numerical approach presented here is particularly fast and efficient on Cartesian component grids. A typical overlapping grid for a region Ω will consist of body fitted curvilinear grids near the boundaries together with one or more background Cartesian grids covering most of the domain. For sufficiently fine grids, the majority of the grid points will reside on the Cartesian grids. In this case, the efficiency of the scheme approaches that of a single Cartesian grid.

The time dependent Maxwell's equations for linear, isotropic and non-dispersive materials are

$$\partial_t \mathbf{E} = \frac{1}{\epsilon}\nabla \times \mathbf{H} - \frac{1}{\epsilon}\mathbf{J}, \tag{1.1}$$

$$\partial_t \mathbf{H} = -\frac{1}{\mu}\nabla \times \mathbf{E}, \tag{1.2}$$

$$\nabla \cdot (\epsilon \mathbf{E}) = \rho, \quad \nabla \cdot (\mu \mathbf{H}) = 0, \tag{1.3}$$

Here $\mathbf{E} = \mathbf{E}(\mathbf{x}, t)$ is the electric field, $\mathbf{H} = \mathbf{H}(\mathbf{x}, t)$ is the magnetic field, $\rho = \rho(\mathbf{x}, t)$ is the electric charge density, $\mathbf{J} = \mathbf{J}(\mathbf{x}, t)$ is the electric current density, $\epsilon = \epsilon(\mathbf{x})$ is the electric permittivity, and $\mu = \mu(\mathbf{x})$ is the magnetic permeability. This first-order system for Maxwell's equations can also be written in a second-order form. By

*Centre for Applied Scientific Computing, Lawrence Livermore National Laboratory, Livermore, CA 94551, henshaw1@llnl.gov. This research was supported under the auspices of the U.S. Department of Energy by the University of California, Lawrence Livermore National Laboratory under contract No. W-7405-Eng-48.

taking the time derivatives of (1.2) and (1.1) and using (1.3) it follows that (see for example [3])

$$\epsilon\mu\ \partial_t^2\mathbf{E} = \Delta\mathbf{E} + \nabla\Big(\nabla\ln\epsilon\ \cdot\mathbf{E}\Big) + \nabla\ln\mu\times\Big(\nabla\times\mathbf{E}\Big) - \mu\partial_t\mathbf{J}, \tag{1.4}$$

$$\epsilon\mu\ \partial_t^2\mathbf{H} = \Delta\mathbf{H} + \nabla\Big(\nabla\ln\mu\ \cdot\mathbf{H}\Big) + \nabla\ln\epsilon\times\Big(\nabla\times\mathbf{H}\Big) + \epsilon\nabla\times(\frac{1}{\epsilon}\mathbf{J}). \tag{1.5}$$

It is evident that the equations for the electric and magnetic field are decoupled with each satisfying a vector wave equation with lower order terms. In the case of constant μ and ϵ and no charges, $\rho = \mathbf{J} = 0$, the equations simplify to the classical second-order wave equations,

$$\partial_t^2\mathbf{E} = c^2\ \Delta\mathbf{E}, \qquad \partial_t^2\mathbf{H} = c^2\ \Delta\mathbf{H} \tag{1.6}$$

where $c^2 = 1/(\epsilon\mu)$. There are some advantages to solving the second-order form of the equations rather than the first-order system. One advantage is that in some cases it is only necessary to solve for one of the variables, say $\mathbf{E}$. If the other variable, $\mathbf{H}$ is required, it can be determined by integrating equation (1.2) as an ordinary differential equation with known $\mathbf{E}$. Alternatively, as a post-processing step $\mathbf{H}$ can be computed from an elliptic boundary value problem formed by taking the curl of equation (1.1). Another advantage of the second-order form, which simplifies the implementation on an overlapping grid, is that there is no need to use a staggered grid formulation. Many schemes approximating the first order system (1.2-1.3) rely on a staggered arrangement of the components of $\mathbf{E}$ and $\mathbf{H}$ such as the popular Yee scheme [41] for Cartesian grids. The development of appropriate boundary conditions is sometimes cited as a disadvatange of solving the second-order form of the equations. The second-order continuous formulation requires additional boundary conditions as discussed in section 2, as well as additional numerical boundary conditions for higher-order accurate discretizations. A primary purpose of this work is to show how to define accurate centered-approximations to the boundary conditions that are based upon compatibility conditions consistent with the governing equations.

There have been a variety of numerical approaches developed for solving the Maxwell's equations in the time-domain and there is extensive literature on the subject including the books by Cohen [6], and Taflove and Hagness [37]. Some references to the different approaches will now be given. One of the most popular approaches is the staggered grid scheme of Yee [41], commonly known as the FDTD (finite-difference time-domain) method. For complex geometry, a *stair-step* approximation to the boundary is often used with the scheme. Improvements to the accuracy of the basic stair-step technique have been considered, by for example, Dey and Mitra [8], and Ditkowski, Dridi and Hesthaven [9]. The Yee scheme has been extended to curvilinear grids, see for example, Lee, Palendech and Mittra [27] and to unstructured grids such as in the DSI (discrete surface-integral) scheme originally developed by Madsen [28] and extended by Gedney [13]. Finite volume methods have been applied to the solution of Maxwell's equations as discussed for example in Holland [22]. Jurgens and Zingg [24] use high-order finite difference approximations on block-structured grids for the equations written as a first-order system. Schemes based on the finite-element-method (FEM) have been developed to solve Maxwell's equations, see for example, Nedelec [29], Jin [23], and Rodrigue and White [33]. The spectral element method has been used by a variety of authors including Yang, Gottlieb and Hesthaven [40]. High-order spectral penalty-methods and discontinuous Galerkin type approaches have also been successful, see for example, Hesthaven and Warburton [21]. Use of hybrid grids, part structured and part unstructured, has become increasingly popular. Rylander and Bondeson [34], for example, present a hybrid FEM-FDTD method that retains the symmetry of the discrete operators, even at the interface between the FEM and FDTD methods. Yee, Chen and Chang [42] considered the solution of Maxwell equations on overlapping grids using a second-order accurate method. Driscoll and Fornberg [10, 11] have developed a block pseudo-spectral method for Maxwell's equations

on two-dimensional overlapping grids. They solve the equations as a first-order system using a high-order difference method on the Cartesian background grid and a pseudo-spectral method on the boundary fitted curvlinear grids.

The **mx** computer code developed as part of this work, is built upon the Overture framework [38]. Grid generation is performed with the Ogen [17] overlapping grid generator which supports the generation of overlapping grids for use with numerical approximations that require wide difference stencils and high-order accurate interpolation at overlapping grid boundaries. High-order accurate methods for overlapping grids have been used previously such as for the shallow water equations by Browning [4] and the incompressible Navier-Stokes equations [16]. The numerical approach developed here is not limited to Maxwell's equations but can potentially be applied to other systems involving second-order wave operators such as the equations of elasticity. The high-order accurate symmetric difference approximations and the techniques presented for developing high-order accurate numerical boundary conditions are applicable more generally.

An overview of the paper now follows. A description of the continuous equations and boundary conditions are presented in section 2. This is followed by a summary of the numerical scheme given in section 3. Overlapping grids are discussed in section 4. In section 5, energy estimates for the second-order formulation are used to motivate the subsequent development of high-order accurate symmetric approximations to the Laplace operator on curvilinear grids. The stability and accuracy of the basic scheme is considered in section 6. In section 7, discrete boundary conditions for material interfaces are devised. These conditions are analysed in section 8, using the Laplace transform and mode analysis. Various aspects of the implementation of the method, including the parallelization of the solver, are considered in section 9. Numerical results in two- and three-dimensions, for the fourth-order accurate version of the scheme, are presented in section 10. Some conclusions are given in the final section 11.

2. Governing Equations and Boundary Conditions. The numerical scheme is based upon the solution of the second-order form of Maxwell's equations. To begin with, the material properties $\epsilon(\mathbf{x})$ and $\mu(\mathbf{x})$ are assumed to be constant. The case of multiple materials will be treated in section 7. In three space dimensions, the initial boundary value problem for Maxwell's equations is then on a domain Ω is given by

$$\partial_t^2 \mathbf{E} = c^2 \, \Delta \mathbf{E}, \qquad \mathbf{x} \in \Omega, \tag{2.1}$$

$$\mathbf{n} \times \mathbf{E} = 0, \;\; \nabla \cdot \mathbf{E} = 0, \qquad \mathbf{x} \in \partial\Omega_E, \quad \text{(PEC B.C.'s)} \tag{2.2}$$

$$\mathcal{B}_F(\mathbf{E}) = 0, \;\; \nabla \cdot \mathbf{E} = 0, \qquad \mathbf{x} \in \partial\Omega_F, \quad \text{(far field B.C.'s)} \tag{2.3}$$

$$\mathbf{E}(\mathbf{x},0) = \mathbf{E}^{(0)}(\mathbf{x}), \quad \mathbf{E}_t(\mathbf{x},0) = \mathbf{E}_t^{(0)}(\mathbf{x}), \qquad \text{(initial conditions)} \tag{2.4}$$

where $\mathbf{E} = (E_x, E_y, E_z)$ and $c = 1/\sqrt{\epsilon\mu}$. The outward normal to the boundary $\partial\Omega$ is $\mathbf{n}$. At a boundary, $\partial\Omega_E$, next to a perfect electrical conductor (PEC), the boundary condition (B.C.) is that the tangential components of the field are zero, $\mathbf{n}\times\mathbf{E} = 0$. For boundaries where the computational domain is truncated, $\partial\Omega_F$, appropriate far-field boundary conditions are applied. The initial conditions should satisfy the constraints $\nabla \cdot \mathbf{E}^{(0)} = 0$ and $\nabla \cdot \mathbf{E}_t^{(0)} = 0$. Note that the second-order formulation requires the additional boundary condition $\nabla \cdot \mathbf{E} = 0$. The fact that Gauss's law, $\nabla \cdot \mathbf{E} = 0$, holds everywhere can be seen by noting that the divergence of the electric field, $\delta = \nabla \cdot \mathbf{E}$, satisfies a second order wave equation, $\delta_{tt} = c^2\Delta\delta$, with zero initial conditions and zero boundary conditions and thus δ will remain identically zero.

In two space dimensions the so-called $\mathrm{TE_Z}$ mode (transverse electric mode with respect to z) is considered. Let $\mathbf{w} = (u, v, w) = (E_x, E_y, H_z)$ denote the vector holding the x- and y-components of the electric field and the z-component of the magnetic field. In addition let $\mathbf{u} = (u, v) = (E_x, E_y)$. The initial-boundary-value problem for

Maxwell's equations in this case is

$$\partial_t^2 \mathbf{w} = c^2 \Delta \mathbf{w} \qquad \mathbf{x} \in \Omega, \tag{2.5}$$

$$\mathbf{u}(\mathbf{x},0) = \mathbf{u}^{(0)}(\mathbf{x}), \quad \mathbf{u}_t(\mathbf{x},0) = \mathbf{u}_t^{(0)}(\mathbf{x}), \quad t = 0, \qquad \text{(initial conditions)} \tag{2.6}$$

$$w(\mathbf{x},0) = w^{(0)}(\mathbf{x}), \quad w_t(\mathbf{x},0) = w_t^{(0)}(\mathbf{x}), \quad t = 0, \qquad \text{(initial conditions)} \tag{2.7}$$

$$\mathbf{n} \times \mathbf{u} = 0, \quad \nabla \cdot \mathbf{u} = 0, \quad \partial_n w = 0, \qquad \mathbf{x} \in \partial\Omega_{\mathrm{E}}, \quad \text{(PEC B.C.'s)} \tag{2.8}$$

$$\mathcal{F}(\mathbf{w}) = 0, \quad \nabla \cdot \mathbf{u} = 0, \qquad \mathbf{x} \in \partial\Omega_F. \quad \text{(far field B.C.'s)} \tag{2.9}$$

As in three-dimensions, the initial conditions should satisfy Gauss' law, $\nabla \cdot \mathbf{u}^{(0)} = 0$, $\nabla \cdot \mathbf{u}_t^{(0)} = 0$. In two-dimensions it may be possible to solve for the one component $w = H_z$ or the two components, $\mathbf{u} = (E_x, E_y)$. However, all three components will be considered here in order to develop the numerical scheme for either case.

3. Summary of the numerical scheme. Consider the second-order wave equation with a forcing function,

$$u_{tt} = c^2 \Delta u + f. \tag{3.1}$$

An attractive time stepping method to solve this second-order wave equation is the *modified equation* approach based on a Taylor series approximation for u_{tt},

$$u(\mathbf{x}, t+\Delta t) - 2u + u(\mathbf{x}, t-\Delta t) = 2\frac{\Delta t^2}{2!}\partial_t^2 u + 2\frac{\Delta t^4}{4!}\partial_t^4 u + 2\frac{\Delta t^6}{6!}\partial_t^6 u + \dots \ .$$

Using the wave equation (3.1) to eliminate even numbers of time derivatives in terms of space derivatives gives

$$\begin{aligned} u(\mathbf{x}, t+\Delta t) - 2u + u(\mathbf{x}, t-\Delta t) = 2\frac{\Delta t^2}{2!}\big(c^2\Delta u + f\big) \ &+ 2\frac{\Delta t^4}{4!}\Big\{(c^2\Delta)^2 u + c^2\Delta f + f_{tt}\Big\} \\ &+ 2\frac{\Delta t^6}{6!}\Big\{(c^2\Delta)^3 u + (c^2\Delta)^2 f + c^2\Delta f_{tt} + \partial_t^4 f\Big\} + \dots \ . \end{aligned} \tag{3.2}$$

This last expansion can be used to derive an approximation of any order that only uses three time levels. Letting $U_{\mathbf{i}}^n \approx u(\mathbf{x}_{\mathbf{i}}, t^n)$ denote a discrete approximation to u at the grid point $\mathbf{x}_{\mathbf{i}}$ and time $t^n = n\Delta t$, a fourth-order accurate approximation is

$$U_{\mathbf{i}}^{n+1} - 2U_{\mathbf{i}}^n + U_{\mathbf{i}}^{n-1} = \Delta t^2\big(c^2\Delta_{4h}U_{\mathbf{i}}^n + f\big) + \frac{\Delta t^4}{12}\big(c^4(\Delta^2)_{2h}U_{\mathbf{i}}^n + c^2\Delta_{2h}f + f_{tt}\big), \tag{3.3}$$

where Δ_{mh} denotes some m^{th}-order approximation to the Laplace operator Δ and $(\Delta^2)_{mh}$ denotes a m^{th}-order approximation to square of the Laplace operator Δ^2. The precise form of these approximations will be given in section 5. Using lower-order approximations for the higher-derivatives prevents the discrete stencil from becoming larger while retaining the order of accuracy. The operators Δ_{4h} and $(\Delta^2)_{2h}$, for example, can be chosen to be 5 points wide in each direction. A sixth-order scheme is

$$\begin{aligned} U_{\mathbf{i}}^{n+1} - 2U_{\mathbf{i}}^n + U_{\mathbf{i}}^{n-1} = \Delta t^2\big(c^2\Delta_{6h}U_{\mathbf{i}}^n + f\big) &+ \frac{\Delta t^4}{12}\big(c^4(\Delta^2)_{4h}U_{\mathbf{i}}^n + c^2\Delta_{4h}f + f_{tt}\big) \\ &+ \frac{\Delta t^6}{360}\big(c^6(\Delta^3)_{2h}U_{\mathbf{i}}^n + c^4(\Delta^2)_{2h}f + c^2\Delta_{2h}f_{tt} + \partial_t^4 f\big). \end{aligned}$$

Higher-order approximations follow easily. The modified equation time-stepping approach is related to the Numerov and Stoermer methods for ODEs [26] and for the the second-order wave equation has been considered by numerous authors, including the work of Dablain [7] and Bell and Shubin [35]. Anné et.al. [1] showed that in one space dimension the time step restriction required for stability is independent of the order

of accuracy. Gustafsson and Mossberg [15] use a similar approach for the treating the equations written as a first order system.

High-order accurate finite difference approximations that use wide stencils require special treatment at boundaries. One common approach for treating approximations near boundaries is to use one-sided difference approximations. Another approach, the one primarily taken here, is to use high-order accurate centered approximations to boundary conditions that use compatibility conditions derived from the continuous formulation [18, 14]. In particular, appropriate compatibility conditions for a PEC boundary are now given. The essential boundary conditions for a perfect electrical conductor are given by equation (2.2). By taking $2m$-time derivatives of these boundary conditions and using equations (2.1) it follows that

$$\mathbf{n} \times (\Delta^m \mathbf{E})(\mathbf{x}, t) = 0, \qquad \nabla \cdot (\Delta^m \mathbf{E})(\mathbf{x}, t) = 0 \qquad \mathbf{x} \in \partial\Omega_E, \tag{3.4}$$

for $m = 0, 1, 2, \ldots$. In the two-dimensional case, taking $2m$-time derivatives of the Neumann boundary condition for H_z leads to the compatibility conditions

$$\partial_n \Delta^m H_z(\mathbf{x}, t) = 0, \qquad \mathbf{x} \in \partial\Omega_E, \tag{3.5}$$

for $m = 0, 1, 2, \ldots$. Discrete approximations to the compatibility conditions (3.4–3.5) can be used as numerical boundary conditions. In general, the use of centered boundary conditions such as those based on these compatibility conditions, will be more stable and more accurate than boundary conditions based on one-sided differences.

In summary, the proposed scheme for Maxwell's equations uses the modified equation time-stepping approximation based on (3.2), such as equation (3.3) for a fourth-order scheme, together with discrete approximations to the boundary conditions (2.2) and compatibility conditions (3.4) or (3.5). These equations are discretized on an overlapping grid. Symmetric difference approximations to the equations are developed in section 5. The solution values at the overlapping grid interpolation points are obtained using high-order accurate interpolation as described in section 4. On a Cartesian grid the basic scheme is neutrally stable and non-dissipative. From an analysis of similar problems [31], it can be expected that such a scheme may develop some weak instabilities near boundaries of curvilinear grids and near interpolation points of the overlapping grid. These instabilities are easily dealt with, however, by the addition of a high-order spatial dissipation. This dissipation does not change the accuracy of the scheme and can be added locally in regions near boundaries and interpolation points. Computational results show that this dissipation has a negligible affect on the overall accuracy of the solution, even for long times.

4. Overlapping Grids. The governing equations for Maxwell's equations are discretized on an overlapping grid $\mathcal{G}$ (see Figures 1 and 11). The overlapping grid consists of a set of component grids, $\mathcal{G} = \{G_g\}$. The component grids overlap and cover the domain Ω. Typically, body fitted curvilinear grids are used near the boundaries while one or more background Cartesian grids are used in the remainder of the domain. Each component grid G_g is a logically rectangular, curvilinear grid in d space dimensions defined by a smooth mapping $\mathbf{x} = \mathbf{G}_g(\mathbf{r})$, from parameter space $\mathbf{r} \in [0, 1]^d$ (the unit-square or unit-cube) to physical space $\mathbf{x} \in \mathbb{R}^d$. This mapping is used to define the location of grid points at any desired resolution. Derivatives of the mapping, $\partial\mathbf{x}/\partial\mathbf{r}$ will appear as coefficients in the discrete approximations, as shown in section 5. Thus, for higher-order approximations it is important that the mapping $\mathbf{G}_g(\mathbf{r})$ be sufficiently smooth to avoid numerical artifacts such as spurious reflections.

Figure 1 shows a simple overlapping grid consisting of two component grids, an annular grid and a background Cartesian grid. The top view shows the overlapping grid while the bottom view shows each grid in parameter space. In this example the annular grid cuts a hole in the Cartesian grid so that the latter grid has a number of unused points that are marked as open circles. The other points on the component grid are marked as discretization points (where the PDE or boundary conditions are discretized) and interpolation points. Solution values at interpolation points are determined by a tensor-product Lagrange interpolant defined in the parameter space

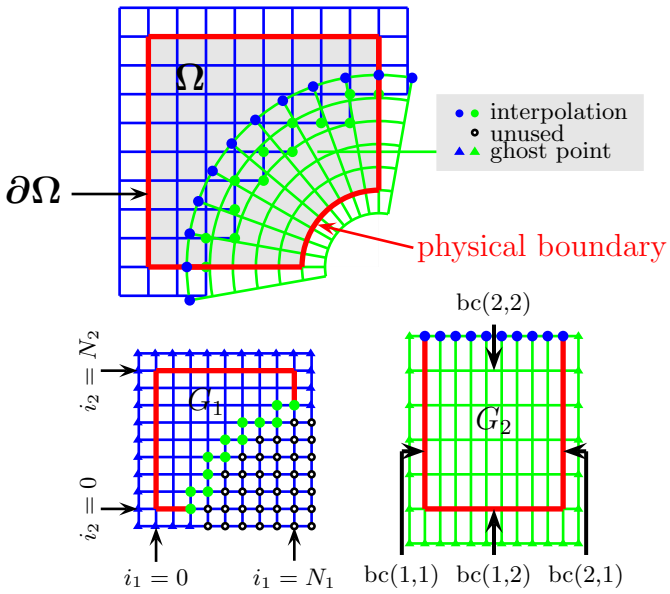

FIG. 1. *The top view shows an overlapping grid consisting of two structured curvilinear component grids. The bottom views show the component grids in the unit square parameter space. Grid points are classified as discretization points, interpolation points or unused points. Ghost points are used to apply boundary conditions.*

of the donor grid, see below for details. Ghost points are used to simplify the discretization of boundary conditions. The grid shown in Figure 1 is appropriate for a second-order method. For a fourth-order approximation with a stencil width of five points, a double fringe of interpolation points is used.

The classification of points on a grid into discretization, unused and interpolation is determined by an overlapping grid generator. In the present case the Ogen grid generator [17] is used. Ogen takes as input a set of overlapping component grids along with a classification of the boundaries of each grid as a physical boundary, an interpolation boundary or a periodic boundary. The algorithm automatically computes the unused points, using physical boundaries to mark points exterior to the domain in a process known as *hole-cutting*, and then determines the discretization points and interpolation points. The grid generator can be used to construct grids for discrete approximations that use wide stencils and that require high-order accurate interpolation.

Each component grid G_g is logically rectangular grid with N_m grid points in each coordinate direction, $m = 1, 2, ..., d$. Let $\mathbf{i} = (i_1, i_2, i_3)$ denote a multi-index, and let $\mathbf{x_i} = \mathbf{G}(\mathbf{r_i})$ denote the grid point corresponding to the unit square coordinate $\mathbf{r_i} = (i_1\Delta r_1, i_2\Delta r_2, i_3\Delta r_3)$ where $i_m = 0, 1, ..., N_m$ and $\Delta r_m = 1/N_m$. Ghost points will correspond to $i_m = -1, -2, ...$ and $i_m = N_m+1, N_m+2, ...$ Introduce a time step Δt, and let $U^n_{\mathbf{i}}$ denote a grid function at time $t^n = n\Delta t$, representing an approximation to $E_x(\mathbf{x_i}, t^n)$, for example. Introduce the standard forward, backward and centered divided difference operators in the r_1 direction by

$$D_{+,r_1}U_{\mathbf{i}} = (U_{i_1+1,i_2,i_3} - U_{\mathbf{i}})/(\Delta r_1), \quad D_{-,r_1}U_{\mathbf{i}} = (U_{\mathbf{i}} - U_{i_1-1,i_2,i_3})/(\Delta r_1),$$
$$D_{0,r_1}U_{\mathbf{i}} = (U_{i_1+1,i_2,i_3} - U_{i_1-1,i_2,i_3})/(2\Delta r_1) \ .$$

Similar definitions hold for difference operators in the other coordinate directions, D_{+,r_m}, D_{-,r_m}, and D_{0,r_m} for $m = 2, 3$. On a Cartesian grid, the grid spacings will be denoted by Δx, Δy and Δz with corresponding difference operators $D_{+,x}$, $D_{-,y}$, $D_{0,z}$ etc.. The difference operators in time are D_{+t}, D_{-t} and $D_{0,t}$ where for example $D_{+t}U^n_{\mathbf{i}} = (U^{n+1}_{\mathbf{i}} - U^n_{\mathbf{i}})/\Delta t$.

The values of the solution at interpolation points (as shown in Figure 1) are determined by a tensor-product Lagrange interpolant, using w points in each direction. Let $\mathbf{x}^{(g)}_{\mathbf{i}}$ denote the coordinates of an interpolation point on grid g and let $\mathbf{r}^d =$

(r_1^d, r_2^d, r_3^d) denote the location of $\mathbf{x}_{\mathbf{i}}^{(g)}$ in the parameter space coordinates of the donor grid $\mathbf{G}_{g_d}$ (i.e. $\mathbf{x}_{\mathbf{i}}^{(g)} = \mathbf{G}_{g_d}(\mathbf{r}^d)$). If $\mathbf{j}$ denotes the lower left corner of the interpolation stencil then the interpolation formula is given by

$$U_{\mathbf{i}}^{(g)} = \sum_{m_1=0}^{\mathrm{w}-1} \sum_{m_2=0}^{\mathrm{w}-1} \sum_{m_3=0}^{\mathrm{w}-1} \alpha_{\mathbf{m}} U_{\mathbf{j}+\mathbf{m}}^{(g_d)} \ . \tag{4.1}$$

where $U_{\mathbf{i}}^{(g)}$ represents the solution value at the interpolation point on grid $\mathbf{G}_g$ and $U_{\mathbf{j}+\mathbf{m}}^{(g_d)}$ the solution values on the *donor* grid $\mathbf{G}_{g_d}$. Here $\mathbf{m} = (m_1, m_2, m_3)$, and the interpolation weights $\alpha_{\mathbf{m}}$ are given by

$$\begin{aligned} \alpha_{\mathbf{m}} &= \mathcal{L}_{m_1}^{\mathrm{w}}(\tilde{r}_1)\ \mathcal{L}_{m_2}^{\mathrm{w}}(\tilde{r}_2)\ \mathcal{L}_{m_3}^{\mathrm{w}}(\tilde{r}_3)\ , \\ \tilde{r}_m &= r_m^i \Delta r_m - j_m\ , \end{aligned}$$

where Δr_m are the parameter space grid spacings on the donor grid and where the Lagrange polynomials $\mathcal{L}_m^{\mathrm{w}}$ are defined in the usual way as

$$\mathcal{L}_m^{\mathrm{w}}(r) = \frac{\prod_{j=0, j\neq m}^{\mathrm{w}-1}(r-j)}{\prod_{j=0, j\neq m}^{\mathrm{w}-1}(m-j)}.$$

For a p^{th}-order approximation to the second-order wave equation, $p = 2, 4, ...$, the width of the interpolation stencil is taken as $\mathrm{w} = p + 1$, following the analysis in [5].

5. High-order accurate symmetric difference approximations on curvilinear grids. In some applications it can be advantageous to use methods that are both high-order accurate and have low dissipation. To achieve these goals it will be helpful to use symmetric difference approximations to the discrete operators that are used in the solution of Maxwell's equations. Standard finite-difference approximations to the Laplace operator on curvilinear grids will not, in general, be symmetric. In this section high-order accurate symmetric difference approximations for general logically rectangular curvilinear grids will be developed.

To understand the relationship between symmetric approximations and low dissipation schemes, consider the solution of the second order wave equation,

$$w_{tt} = \nabla \cdot (c^2 \nabla w), \tag{5.1}$$

for the function $w = w(\mathbf{x}, t)$ on a periodic domain $\Omega = [0, 2\pi]^d$. Let $(u, v) = \int_\Omega u^* v \ d\mathbf{x}$ and $\|u\| = (u, u)^{1/2}$ denote the usual L_2 inner product and norm on this domain. The wave equation (5.1) has no dissipation and there is an "energy" that remains constant over time. This energy can be determined by multiplying the equation by w_t, integrating over the domain and using integration by parts, giving

$$\frac{1}{2}\partial_t \left\{ \|w_t\|^2 + \|c\nabla w\|^2 \right\} = 0 \ .$$

The "energy" $\mathcal{E} = \|w_t\|^2 + \|c\nabla w\|^2$ is thus constant on a periodic domain. Discrete approximations to the wave equation (5.1) will not in general have a discrete energy that remains constant. For stability reasons many approximations will have some dissipation built into the spatial approximation or into the time stepping method. There are, however, a class of stable methods with no dissipation. Consider, for example, the second-order accurate centered approximation

$$D_{+t}D_{-t}W_{\mathbf{i}}^n = (D_{+,x}D_{-,x} + D_{+,y}D_{-,y})W_{\mathbf{i}}^n, \tag{5.2}$$

for use on a Cartesian grid, where $W_{\mathbf{i}}^n \approx w(\mathbf{x}_i, t^n)$. Let $(U, V)_h = \sum_{\mathbf{i}} U_{\mathbf{i}}^* V_{\mathbf{i}}\ \Delta x_1 \Delta x_2$ and $\|U\|_h = (U, U)_h^{1/2}$ denote the discrete L_2 inner product and norm on the Cartesian grid where the sum is over the grid points $i_m = 0, 1, ..., N_m - 1$. Equation (5.2) has a discrete "energy" $\mathcal{E}_h = \|D_{-t}W^n\|_h^2 + (D_{-x}W^n, D_{-x}W^{n-1})_h + (D_{-y}W^n, D_{-y}W^{n-1})_h$,

that is conserved, as will be shown below. Equation (5.2) is a special case of the more general discrete approximation

$$D_{+t}D_{-t}W^n = AW^n, \qquad n = 2,3,4,..., \tag{5.3}$$

$$W^0 = W^{(0)}, \quad W^1 = W^{(1)}, \quad \text{(initial conditions)}, \tag{5.4}$$

where $W^n \in \mathbb{R}^N$ is the vector of all N grid point values $W^n_{\mathbf{i}}$, and $A \in \mathbb{R}^{N\times N}$ is the matrix representing the spatial discretization (including eliminated boundary conditions). The three-level time stepping schemes used in this paper are of this form (although for solutions on general overlapping grids a high-order dissipation is also added, section 9.2). The following lemma indicates the conditions on A so that all solutions to (5.3) remain uniformly bounded in time.

LEMMA 5.1. *The scheme* (5.3) *is stable (the solutions remain uniformly bounded for all n) if and only if A has a complete set of eigenvectors, the eigenvalues* λ *of A are real and negative and* Δt *satisfies* $-4 < \lambda\Delta t^2 < 0$ *for all* λ.

Proof. Suppose that $\widehat{V}$ is an eigenvector of A corresponding to the eigenvalue λ. Looking for a solution of the form $V^n = \kappa^n\widehat{V}$ implies that κ satisfies the characteristic equation $\kappa - 2 + \kappa^{-1} = \lambda\Delta t^2$ with

$$\kappa = 1 + \frac{1}{2}\lambda\Delta t^2 \pm \sqrt{(1+\frac{1}{2}\lambda\Delta t^2) - 1}. \tag{5.5}$$

When $\lambda = 0$ ($\kappa = 1$) or $\lambda\Delta t^2 = -4$ ($\kappa = -1$) there is a double root and the solutions can grow linearly in time,

$$V^n = (c_0 + c_1(n\Delta t))\widehat{V}, \qquad \text{for } \lambda = 0,$$
$$V^n = (-1)^n\ (c_0 + c_1(n\Delta t))\widehat{V}, \quad \text{for } \lambda\Delta t^2 = -4.$$

Therefore in these two cases the solutions will not be uniformly bounded for general initial conditions. A root, κ, of the characteristic equation will be a simple root and satisfy $|\kappa| = 1$ if and only if λ is real and

$$-4 < \lambda\Delta t^2 < 0. \tag{5.6}$$

In this case the solution will be of the form

$$V^n = (c_0\kappa^n + c_1\kappa^{-n})\widehat{V},$$

and will remain uniformly bounded. If λ is not real or $\lambda > 0$ or $\lambda\Delta t^2 < -4$ there will be one root with $|\kappa| > 1$ and the approximation (5.3) is not uniformly bounded. If all λ satisfy (5.6) and there is a complete set of eigenvectors then the general solution can be represented as a linear combination of the eigenvectors and this solution will remain uniformly bounded. If there is not a complete set of eigenvectors then the Jordan normal form of A has a Jordan block of size larger than 1. In this case there are solutions of the form $V^n = (n\Delta t)\kappa^n$ and hence the solutions do not remain bounded in this case. □

The conditions of lemma 5.1 will be satisfied when A is symmetric and the eigenvalues of A are less than zero. In this case a discrete energy estimate can be obtained as follows. Taking the inner product of $W^{n+1} - W^{n-1}$ with equation (5.3) and rearranging terms gives

$$\frac{1}{\Delta t^2}|W^{n+1} - W^n|^2 - \langle W^{n+1}, AW^n\rangle = \frac{1}{\Delta t^2}|W^n - W^{n-1}|^2 - (W^n, AW^{n-1}\rangle.$$

Therefore the quantity

$$\mathcal{E}^n_h = \frac{1}{\Delta t^2}|W^n - W^{n-1}|^2 - \langle W^n, AW^{n-1}\rangle \tag{5.7}$$

$$= \frac{1}{\Delta t^2}\left\langle D_{+t}W^{n-1}, \big(I + \frac{\Delta t^2}{4}A\big)D_{+t}W^{n-1}\right\rangle - \langle W^{n-\frac{1}{2}}, AW^{n-\frac{1}{2}}\rangle \tag{5.8}$$

remains constant for all time, where $W^{n-\frac{1}{2}} := (W^n + W^{n-1})/2$. It can be seen from (5.8) that $\mathcal{E}_h^n$ is positive provided Δt satisfies the bound (5.6) for all eigenvalues of A (see Kreiss et.al [25] or Cohen [6] for further details).

The above results provide a motivation for developing symmetric difference approximations for discretizations of Maxwell's equations. To this end, consider the generalized Laplace operator, L defined by

$$Lw = \nabla \cdot (k \nabla w) \ . \tag{5.9}$$

A straight-forward approach to discretize L on a curvilinear grid is to use the mapping method, as follows. Using the chain rule, the operator L can be written in general curvilinear coordinates (with summation convention) as

$$Lw = k(\mathbf{r}) \frac{\partial r_n}{\partial x_i} \frac{\partial r_m}{\partial x_i} \frac{\partial^2 w}{\partial r_m \partial r_n} + \frac{\partial r_n}{\partial x_i} \Big\{ k(\mathbf{r}) \frac{\partial}{\partial r_n} \Big(\frac{\partial r_m}{\partial x_i} \Big) + \frac{\partial k}{\partial r_n} \frac{\partial r_m}{\partial x_i} \Big\} \frac{\partial w}{\partial r_m}. \tag{5.10}$$

The metric terms $\partial r_m / \partial x_n$ are computed from the mapping that defines the grid and are thus assumed to be known. The derivatives with respect to the parameter space coordinates r_m can be approximated with standard central difference approximations. For example, a fourth-order approximation to (5.10), denoted by FD4, will use

$$\begin{aligned}
\frac{\partial^2}{\partial r_m^2} &\approx D_{+,r_m} D_{-,r_m} \Big(I - \frac{\Delta r_m^2}{12} D_{+,r_m} D_{-,r_m} \Big), \\
\frac{\partial}{\partial r_m} &\approx D_{4,r_m} \equiv D_{0,r_m} \Big(I - \frac{\Delta r_m^2}{6} D_{+,r_m} D_{-,r_m}, \Big), \\
\frac{\partial^2}{\partial r_m \partial r_n} &\approx D_{4,r_m} D_{4,r_n} \quad (m \neq n).
\end{aligned}$$

Finite difference approximations FDm of order m for $m = 2, 4, 6, ...$ can be defined in this way. The resulting approximations will not, however, be symmetric on general curvilinear grids. In the remainder of this section, it will be shown how to construct high-order accurate symmetric approximations to L for arbitrary curvilinear grids.

The operator L can be written in *conservation* form, or *self-adjoint form*, in general curvilinear coordinates as

$$Lw = \frac{1}{J} \sum_{m=1}^{d} \sum_{n=1}^{d} \frac{\partial}{\partial r_m} \left(A^{mn} \frac{\partial w}{\partial r_n} \right), \tag{5.11}$$

$$A^{mn} = kJ \sum_{\mu=1}^{d} \sum_{\nu=1}^{d} \frac{\partial r_m}{\partial x_\mu} \frac{\partial r_n}{\partial x_\nu}, \tag{5.12}$$

where J denotes the determinant of the Jacobian matrix $[\partial x_i / \partial r_j]$. To improve readability in the subsequent discussion let $(r, s) = (r_1, r_2)$ and $(h_r, h_s) = (\Delta r_1, \Delta r_2)$. The discrete inner product on a curvilinear grid is defined as

$$(U_{\mathbf{i}}, V_{\mathbf{i}})_h = \sum_{\mathbf{i}} U_{\mathbf{i}}^* V_{\mathbf{i}} \ J_{\mathbf{i}} \ h_r h_s \ . \tag{5.13}$$

Consider approximations to the two operators, $\mathcal{L}_{rr} = \partial_r (a \partial_r)$ and $\mathcal{L}_{rs} = \partial_r (b \partial_s)$ that are representative of the terms appearing in the expression (5.11) for L. The operator $\mathcal{L}_{rr}$ will be approximated in the discrete form

$$\mathcal{L}_{rr} w = \partial_r (a \partial_r w) \approx \mathcal{D}_+ (\tilde{a}_{i-\frac{1}{2}} \mathcal{D}_-) w(\mathbf{r_i}),$$

where $\mathcal{D}_+ \approx \partial_r w(r + h_r/2)$ and $\mathcal{D}_- \approx \partial_r w(r - h_r/2)$ are some appropriately defined high-order accurate approximations to the derivatives at locations midway between grid points. To simplify notation let $D_+ = D_{+,r}$ and $D_- = D_{-,r}$. An order $2m + 2$ approximation for $\mathcal{D}_+$ is obtained from the expansion

$$\frac{\partial u}{\partial r}(r + h_r/2) = D_+ \left[1 + \sum_{n=1}^{m} \alpha_n h_r^{2n} (D_+ D_-)^n \right] w(r + h_r/2) + \mathcal{O}(h_r^{2m+2}), \tag{5.14}$$

where the coefficients α_i can be determined from equating coefficients in the expression $y = \sin(y)\left[1 + \sum_{n=1}^{\infty} \alpha_n (-4\sin^2(y))^n\right]$, (see for example [12] or [14]). The first four values of α_i are given by

$$\alpha_1 = -\frac{1}{6}, \qquad \alpha_2 = \frac{3}{640}, \qquad \alpha_3 = -\frac{5}{7168}, \qquad \alpha_4 = \frac{35}{294912} \ .$$

Assuming that the coefficient $a(r)$ is given at the grid points, a_i, approximations to $a_{i-1/2}$ will be needed. These approximations can be obtained by interpolation in a straight-forward fashion and to order $m = 2, 4, 6$, are given by

$$\begin{aligned} a^{(2)}_{i-1/2} &= \frac{1}{2}(a_i + a_{i-1}), \quad a^{(4)}_{i-1/2} = \frac{9}{16}(a_i + a_{i-1}) - \frac{1}{16}(a_{i+1} + a_{i-2}), \\ a^{(6)}_{i-1/2} &= \frac{75}{128}(a_i + a_{i-1}) - \frac{25}{256}(a_{i+1} + a_{i-2}) + \frac{3}{16}(a_{i+2} + a_{i-3}), \end{aligned}$$

where $a^{(m)}_{i-1/2} = a_{i-1/2} + O(h_r^m)$. Note that other forms of interpolation may be appropriate when the coefficient k is discontinuous. Define $\mathcal{D}_+$ and $\mathcal{D}_-$ as

$$\mathcal{D}_\pm = D_\pm \left[1 + \sum_{n=1}^{\infty} \alpha_n h_r^{2n} (D_+ D_-)^n\right] \ .$$

Expanding the expression $\mathcal{D}_+(a\mathcal{D}_-)$ in powers of h_r^2 leads to

$$\begin{aligned} \frac{\partial}{\partial r}\left(a\frac{\partial}{\partial r}\right) &= D_+(a^{(m)}_{i-1/2} D_-) - \frac{h_r^2}{24}\left[D_+(a^{(m-2)}_{i-1/2} D_+ D_-^2) + D_+^2 D_-(a^{(m-2)}_{i-1/2} D_-)\right] \\ &+ \frac{h_r^4}{24^2}\left[D_+^2 D_-(a^{(m-4)}_{i-1/2} D_+ D_-^2)\right] + \frac{3h_r^4}{640}\left[D_+(a^{(m-4)}_{i-1/2} D_+^2 D_-^3) + D_+^3 D_-^2(a^{(m-4)}_{i-1/2} D_-)\right] \\ &- \frac{5h_r^6}{7168}\left[D_+^4 D_-^3(a^{(m-6)}_{i-1/2} D_-) + D_+(a^{(m-6)}_{i-1/2} D_+^3 D_-^4)\right] \\ &- \frac{3h_r^6}{640\cdot 24}\left[D_+^2 D_-(a^{(m-6)}_{i-1/2} D_+^2 D_-^3) + D_+^3 D_-^2(a^{(m-6)}_{i-1/2} D_+ D_-^2)\right] + O(h_r^8) \end{aligned} \tag{5.15}$$

Note that different orders of approximation for $a_{i-1/2}$ are used, so that the difference stencil for a m^{th}-order formulation is no larger than $m+1$ points wide in each direction. Equation (5.15) can be used to generate symmetric approximations of order m by involving terms up to and including those of order h_r^m. For example, a fourth-order symmetric approximation to $J^{-1}\partial_r(a\partial_r)$ is

$$\mathcal{L}^{(4)}_{rr}[a]w := \frac{1}{J_{\mathbf{i}}}\Big\{D_+(a^{(4)}_{i-1/2} D_-) - \frac{h_r^2}{24}\left[D_+(a^{(2)}_{i-1/2} D_+ D_-^2) + D_+^2 D_-(a^{(2)}_{i-1/2} D_-)\right]\Big\} w,$$

while a sixth-order symmetric approximation is

$$\begin{aligned} \mathcal{L}^{(6)}_{rr}[a]w := \frac{1}{J_{\mathbf{i}}}\Big\{ & D_+(a^{(6)}_{i-1/2} D_-) - \frac{h_r^2}{24}\left[D_+(a^{(4)}_{i-1/2} D_+ D_-^2) + D_+^2 D_-(a^{(4)}_{i-1/2} D_-)\right] \\ & + \frac{h_r^4}{24^2}\left[D_+^2 D_-(a^{(2)}_{i-1/2} D_+ D_-^2)\right] + \frac{3h_r^4}{640}\left[D_+(a^{(2)}_{i-1/2} D_+^2 D_-^3) + D_+^3 D_-^2(a^{(2)}_{i-1/2} D_-)\right]\Big\} w \ . \end{aligned}$$

It is easy to show that the approximations, $\mathcal{L}^{(4)}_{rr}[a]$ and $\mathcal{L}^{(6)}_{rr}[a]$ are symmetric since the adjoint of $J^{-1}D_+$ is $-J^{-1}D_-$ and the adjoint of $J^{-1}D_{-1}$ is $-J^{-1}D_+$ (with respect to the discrete inner product (5.13)).

The operator $\mathcal{L}_{rs} = \partial_r(b\partial_s)$ for the mixed derivative terms, is approximated using

$$\frac{\partial}{\partial r}\left(b\frac{\partial}{\partial s}\right) \approx D_{0r}\left[1 + \sum_{n=1}^{\infty} \beta_n h_r^{2n} (D_{+r} D_{-r})^n\right]\Big\{bD_{0s}\left[1 + \sum_{n=1}^{\infty} \beta_n h_s^{2n} (D_{+s} D_{-s})^n\right]\Big\},$$

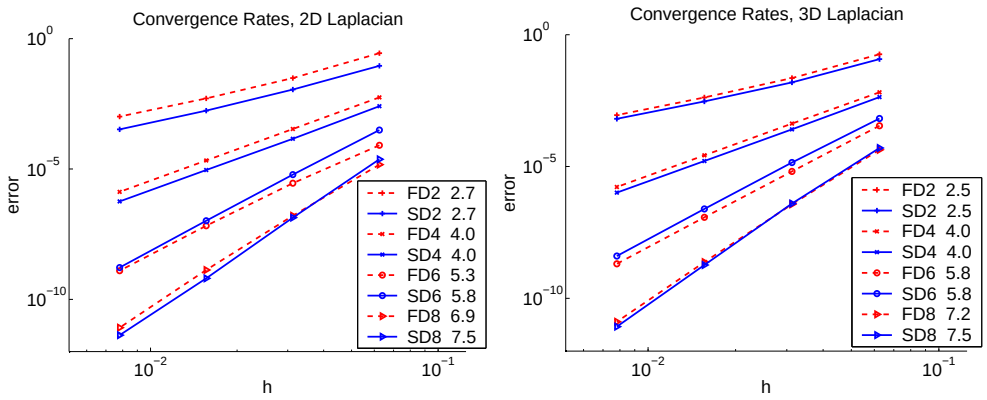

FIG. 2. *Convergence rates for the errors in computing the Laplacian on a smooth non-orthogonal grid. FDm denotes the standard finite difference approximations of order m while SDm denotes the symmetric difference approximations of order m. The estimated convergence rate for each approximation is indicated in the legend.*

where $D_{+r} = D_{+,r_1}$, $D_{+s} = D_{+,r_2}$ etc.. and where $b = b_{\mathbf{i}}$ denotes the value of b at a grid point. The expression can be expanded as

$$\begin{aligned}\frac{\partial}{\partial r}\left(b\frac{\partial}{\partial s}\right) &= D_{0r}(bD_{0s}) - \frac{1}{6}\left[h_s^2 D_{0r}(bD_{0s}D_{+s}D_{-s}) + h_r^2 D_{0r}D_{+r}D_{-r}(bD_{0s})\right] \\ &+ \frac{1}{30}\left[h_s^4 D_{0r}(bD_{0s}D_{+s}^2D_{-s}^2) + h_r^2 D_{0r}D_{+r}^2D_{-r}^2(bD_{0s})\right] \\ &+ \frac{1}{6\cdot 6}h_r^2h_s^2\left[D_{0r}D_{+r}D_{-r}(bD_{0s}D_{+s}D_{-s})\right] \\ &- \frac{1}{140}\left[h_s^6 D_{0r}(bD_{0s}D_{+s}^3D_{-s}^3) + h_r^6 D_{0r}D_{+r}^3D_{-r}^3(bD_{0s})\right] \\ &- \frac{1}{6\cdot 30}\left[h_r^2h_s^4 D_{0r}D_{+r}D_{-r}(bD_{0s}D_{+s}^2D_{-s}^2)\right. \\ &\qquad \left. + h_r^4h_s^2 D_{0r}D_{+r}^2D_{-r}^2(bD_{0s}D_{+s}D_{-s})\right] + O(h_r^8, h_s^8)\ . \end{aligned} \tag{5.16}$$

In this case the values of b that appear are located at the grid points and no interpolation is needed. From (5.16), a fourth order approximation to $J^{-1}\partial_r(b\partial_s)$ is

$$\mathcal{L}_{rs}^{(4)}[b]w := \frac{1}{J_{\mathbf{i}}}\Big\{D_{0r}(bD_{0s}) - \frac{1}{6}\left[h_s^2 D_{0r}(bD_{+s}D_{-s}D_{0s}) + h_r^2 D_{0r}D_{+r}D_{-r}(bD_{0s})\right]\Big\}w.$$

This operator is not symmetric, but the combination $\mathcal{L}_{rs}^{(4)}[b]+\mathcal{L}_{sr}^{(4)}[b]$ will be symmetric. A fourth-order symmetric approximation to $L = \nabla\cdot(k\nabla)$ denoted by $\mathcal{L}^{(4)}$ is thus

$$\mathcal{L}^{(4)} = \sum_{m=1}^{d}\sum_{n=1}^{d}\mathcal{L}_{r_m r_n}^{(4)}[A^{mn}]\ .$$

where the coefficients A^{mn} are defined by (5.12). The symmetric approximation can be easily generalized to the case where $k(\mathbf{x})$ is replaced by a symmetric tensor; this only changes the definition of A^{mn}.

The symmetric approximations have been implemented in two and three space dimensions for orders $m = 2, 4, 6, 8$. Figure 2 compares the accuracy of the symmetric difference operators of order m, denoted by SDm to those of the standard finite difference operators of order m, denoted by FDm. The errors in computing the Laplacian of a trigonometric function on a smooth non-orthogonal grid are presented in the figure for a sequence of grids of increasing resolution. The estimated convergence rate for each approximation is also indicated. These estimated rates are computed from a least squares fit to the log of the error versus the log of the grid spacing. The results show that the symmetric schemes SDm have similar errors to the finite difference schemes FDm. The convergence rates are reasonably close to the expected

values. Note that the numerical values of the computed rates are sensitive to small changes in the data.

To illustrate that the discrete operators SDm are indeed symmetric on arbitrary logically-rectangular grids, a computation was performed on the grid shown in Figure 3. The grid for the unit square, with periodic boundary conditions, is obtained by randomly perturbing the grid points of a Cartesian grid. The grid points are defined as $\mathbf{x_i} = ((i_1 + \mathcal{R}^{(x)}/4)\Delta x, (i_2 + \mathcal{R}^{(y)}/4)\Delta y)$ where $\mathcal{R}^{(x)}$ and $\mathcal{R}^{(y)}$ are pseudo-random numbers uniformly distributed in $[-1, 1]$. Figure 3 shows the results from computations solving Maxwell's equations with $c = 1$ on a two-dimensional perturbed square. The discrete energy (5.7) for the component E_x (other components are similar) is plotted for different schemes for $t \in [0, 100]$. Let the symmetric time-stepping schemes be denoted by TnSDm where n is the order of accuracy in time and m is the order of accuracy in space. Figure 3 presents results for the methods T2SD2, T4SD4, T2SD6 and T2SD8. The scheme T4SD4 is given by equation (3.3). The schemes T2SDm use second-order accurate time stepping with an m^{th} order accurate approximation to the Laplacian, $U^{n+1}_{\mathbf{i}} - 2U^n_{\mathbf{i}} + U^{n-1}_{\mathbf{i}} = \Delta t^2 c^2 \Delta_{mh} U^n_{\mathbf{i}}$. The discrete energy is essentially constant over the computation (to within a relative error of about 10^{-10} in 64 bit double precision) for all schemes that use the symmetric operators. By comparison, schemes using the standard finite difference approximations, denoted by TmFDn are not energy preserving. These schemes are not stable for this grid without the addition of some dissipation. Figure 3 also shows the corresponding results for a perturbed three-dimensional box.

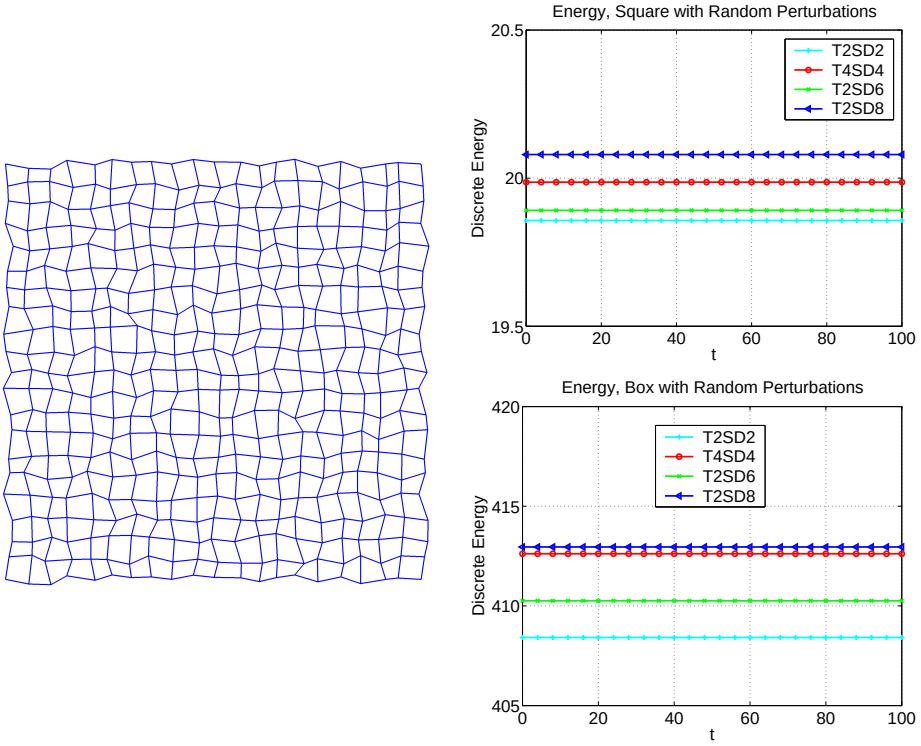

FIG. 3. *The computation of Maxwell's equations on a randomly perturbed Cartesian grid using the symmetric approximations. The discrete energy remains almost constant (to a relative error of about 10^{-10} in double precision) using the symmetric difference approximations, even on a non-smooth, non-orthognal grid. Results for a perturbed grid for a square and a perturbed grid for a box are shown for the various schemes TmSDn of order of accuracy n in time and m in space.*

6. Analysis of the scheme. In this section the stability of the fourth-order accurate time stepping scheme and boundary conditions is analyzed for a model problem. The analysis considers the solution to Maxwell's equations on the unit square, $\Omega = (0, 1)^2$, with PEC boundary conditions at $x = 0$ and $x = 1$ and periodic boundary conditions in y. A Cartesian grid is introduced with mesh points $\mathbf{x_i} = (x_i, y_j) = (i\Delta x, j\Delta y)$, where $\mathbf{i} = (i, j)$ and $i = -2, 1, 0, 1, 2, ..., N_1, N_1 + 1, N_1 + 2$

with $\Delta x = 1/N_1$, and $j = 0, 1, 2, ..., N_2 - 1$, with $\Delta y = 1/N_2$. Two lines of ghost points have been introduced outside the boundaries at $x = 0$ and $x = 1$. Discrete approximations to $E_x(\mathbf{x_i}, t^n)$ and $E_y(\mathbf{x_i}, t^n)$ are given by U_{ij}^n and V_{ij}^n, respectively, with $\mathbf{U_i^n} = (U_{\mathbf{i}}^n, V_{\mathbf{i}}^n)$. For this two-dimensional example the discretization for the magnetic field will not be presented since it is the same as the discretization for E_x. The interior equations (2.5) are discretized in a fourth-order manner using the modified equation approximation (3.3)

$$\mathbf{U_i^{n+1}} - 2\mathbf{U_i^n} + \mathbf{U_i^{n-1}} = (c\Delta t)^2 \Delta_{4h} \mathbf{U_i} + \frac{(c\Delta t)^4}{12} \Delta_{2h}^2 \mathbf{U_i}, \quad \text{for } \; i = 0, 1, ..., N_1, j = 0, 1, .., N_2 - 1. \tag{6.1}$$

Here Δ_{4h} is a fourth-order approximation to Δ and Δ_{2h}^2 is a second-order approximation to Δ^2 given by

$$\Delta_{4h} \equiv D_{+,x} D_{-,x} \big(1 - \frac{\Delta x^2}{12} D_{+,x} D_{-,x}\big) + D_{+,y} D_{-,y} \big(1 - \frac{\Delta y^2}{12} D_{+,y} D_{-,y}\big),$$
$$\Delta_{2h}^2 \equiv \big(D_{+,x} D_{-,x} + D_{+,y} D_{-,y}\big)^2.$$

The divided difference operators $D_{+,x}$, $D_{-,x}$, D_{0x} etc. were defined in section 4. The boundary conditions at $x = 0$ ($i = 0$) and $x = 1$ ($i = N_1$) are discretized as

$$V_{\mathbf{i}} = 0, \qquad \text{for } i = 0, N_1, \tag{6.2}$$

$$D_{0x} \big(1 - \frac{\Delta x^2}{6} D_{+,x} D_{-,x}\big) U_{\mathbf{i}} = 0, \qquad \text{for } i = 0, N_1, \tag{6.3}$$

$$D_{+,x} D_{-,x} \big(1 - \frac{\Delta x^2}{12} D_{+,x} D_{-,x}\big) V_{\mathbf{i}} = 0, \qquad \text{for } i = 0, N_1, \tag{6.4}$$

$$D_{0x} D_{+,x} D_{-,x} U_{\mathbf{i}} = 0, \qquad \text{for } i = 0, N_1, \tag{6.5}$$

$$\big(D_{+,x} D_{-,x}\big)^2 V_{\mathbf{i}} = 0, \qquad \text{for } i = 0, N_1, \tag{6.6}$$

where three additional *numerical boundary conditions* have been introduced. The boundary conditions (6.2-6.6) are, respectively, approximations to $E_y = 0$, fourth-order approximations to $\nabla \cdot \mathbf{E} = 0$, $\Delta E_y = 0$, and second-order approximations to $\nabla \cdot \Delta \mathbf{E} = 0$ and $\Delta^2 E_y = 0$. The latter three equations arise from the compatibility conditions (3.4). The scheme is completed by specifying initial values for two time levels, for example,

$$\mathbf{U_{ij}^0} = \mathbf{E}^{(0)}(\mathbf{x}_{ij}), \tag{6.7}$$

$$\mathbf{U_{ij}^1} = \mathbf{E}^{(0)}(\mathbf{x}_{ij}) + \Delta t \mathbf{E}_t^{(0)}(\mathbf{x}_{ij}) + \frac{\Delta t^2}{2} \Delta_{2h} \mathbf{E}^{(0)}(\mathbf{x}_{ij}) + \frac{\Delta t^3}{3!} \Delta_{2h} \mathbf{E}_t^{(0)}(\mathbf{x}_{ij}). \tag{6.8}$$

LEMMA 6.1. *The solution to the discrete approximation to the vector wave equation* (6.1) *with boundary conditions (6.2-6.6) is stable (the solutions remain uniformly bounded) provided*

$$\Delta t < c^{-1} \left(\frac{1}{\Delta x^2} + \frac{1}{\Delta y^2} \right)^{-1/2}. \tag{6.9}$$

Proof. Making the ansatz $\widetilde{U}_{\mathbf{i}}^n = \kappa^n \cos(\pi m x_i) e^{i 2\pi n y_j}$ and $\widetilde{V}_{\mathbf{i}}^n = \kappa^n \sin(\pi m x_i) e^{i 2\pi n y_j}$ it follows that $\widetilde{U}_{\mathbf{i}}^n$, and $\widetilde{V}_{\mathbf{i}}^n$ satisfy equations (6.1) and boundary conditions (6.2-6.6) provided κ satisfies the characteristic equation

$$\kappa - 2 + \kappa^{-1} = -4G \tag{6.10}$$

where

$$G = \lambda_x^2 \sigma_x [1 + \frac{1}{3} \sigma_x] + \lambda_y^2 \sigma_y [1 + \frac{1}{3} \sigma_y] - \frac{1}{3} [\lambda_x^2 \sigma_x + \lambda_y^2 \sigma_y]^2,$$
$$\sigma_x = \sin^2(\xi_x/2), \quad \sigma_y = \sin^2(\xi_y/2),$$
$$\lambda_x = c \frac{\Delta t}{\Delta x}, \quad \lambda_y = c \frac{\Delta t}{\Delta y}, \quad \xi_x = \pi m \Delta x, \quad \xi_y = 2\pi n \Delta y,$$
$$m = 0, 1, 2, ..., N_1, \quad n = 0, 1, 2, ..., N_2 - 1.$$

The two roots of the characteristic equation (6.10) are $\kappa_\pm = (1-2G) \pm \sqrt{(1-2G)^2 - 1}$ where $\kappa_+ = \kappa_-^{-1}$. The roots will satisfy $|\kappa_\pm| = 1$ and the solutions will remain uniformly bounded provided $0 < G < 1$ (following the argument in the proof of lemma 5.1). Letting $\gamma = \lambda_x^2\sigma_x + \lambda_y^2\sigma_y$ it follows that G can be written in the form

$$\begin{aligned} G &= \gamma - \frac{1}{3}\gamma^2 + \frac{1}{3}(\lambda_x^2\sigma_x^2 + \lambda_y^2\sigma_y^2), \\ &\le \gamma - \frac{1}{3}\gamma^2 + \frac{1}{3}(\lambda_x^2\sigma_x + \lambda_y^2\sigma_y) \ = \gamma + \frac{1}{3}\gamma(1-\gamma). \end{aligned}$$

The function G is always positive for $0 < \gamma < 1$. The function $\widetilde{G}(\gamma) = \gamma + \frac{1}{3}\gamma(1-\gamma)$ is less than 1 for $0 < \gamma < 1$ and thus $0 < G < 1$ provided $\gamma < 1$. Therefore the condition that $\widetilde{U}_{\mathbf{i}}^n$ and $\widetilde{V}_{\mathbf{i}}^n$ remain uniformly bounded is

$$\lambda_x^2\sigma_x + \lambda_y^2\sigma_y \le \lambda_x^2 + \lambda_y^2 < 1, \tag{6.11}$$

Let $\kappa_{m,n}$ and $G_{m,n}$ denote the values of κ_+ and G as functions of m and n. The general solution can be written as

$$\begin{aligned} U_{\mathbf{i}}^n &= \sum_m \sum_n (A_{m,n}\kappa_{m,n}^n + B_{m,n}\kappa_{m,n}^{-n}) \cos(mx_{\mathbf{i}}) e^{iny_{\mathbf{i}}}, \\ V_{\mathbf{i}}^n &= \sum_m \sum_n (C_{m,n}\kappa_{m,n}^n + D_{m,n}\kappa_{m,n}^{-n}) \sin(mx_{\mathbf{i}}) e^{iny_{\mathbf{i}}}, \end{aligned}$$

where the values of $A_{m,n}$, $B_{m,n}$, $C_{m,n}$ and $D_{m,n}$ are determined by the initial conditions. The solution will be stable provided $0 < G_{m,n} < 1$ for all permissible m, n. It follows from the stability condition (6.11) and the definitions of λ_x and λ_y that the solution to the model problem is stable provided the time step satisfies (6.9). $\square$.

Note that

$$\kappa_{mn} = 1 + ik\Delta t + \frac{1}{2}(ik)^2 + \frac{1}{3!}(ik)^3 + \frac{1}{4!}(ik)^4 + O(\Delta t h^4, \Delta t^3 h^2, \Delta t^5)$$

where $h = \sqrt{\Delta x^2 + \Delta y^2}$, $k = \sqrt{k_x^2 + k_y^2}$, $k_x = \pi m$, and $k_y = 2\pi n$. This shows that κ_{mn} is a fourth-order accurate approximation to $e^{ik\Delta t}$. The discrete eigenfunctions $\widetilde{U}_{\mathbf{i}}^n$ and $\widetilde{V}_{\mathbf{i}}^n$ are thus fourth-order accurate approximations to the eigenfunctions of the continuous problem, and it is apparent that the discrete approximation to the model problem is fourth-order accurate.

In three dimensions an argument similar to that used for the two-dimensional case shows that the stability condition is

$$\Delta t < c^{-1} \left(\frac{1}{\Delta x^2} + \frac{1}{\Delta y^2} + \frac{1}{\Delta z^2} \right)^{-1/2}. \tag{6.12}$$

7. Boundary conditions at material interfaces. In this section the propagation of electromagnetic waves through different dielectric (insulating) materials will be considered. The domain Ω is partitioned into a set of sub-domains, $\Omega = \bigcup_k \Omega_k$, with each Ω_k representing a region with different material properties,

$$\epsilon(\mathbf{x}) = \epsilon_k, \quad \mu(\mathbf{x}) = \mu_k, \quad \text{for } \mathbf{x} \in \Omega_k.$$

The assumption is made that ϵ and μ are constant within each sub-domain (although this restriction is not essential). The boundaries of each sub-domain, $\partial\Omega_k$, are assumed to be sufficiently smooth so that normal and tangent vectors to the interface can be defined. Overlapping grids will be used to discretize each sub-domain separately. The sub-domain boundaries will be represented with boundary fitted grids (see for example Figure 10). Maxwell's equations in second-order form are discretized in each sub-domain using the high-order accurate difference approximations discussed in previous sections. Ghost points are used on the grids on both sides of the interface as shown in

the one-dimensional overlapping grid of Figure 4. Boundary conditions at the interface are required for the numerical approximation. These boundary conditions are used to determine the solution values at the ghost points. As in the case of the PEC boundary, centered numerical boundary conditions are developed from compatibility conditions consistent with the governing equations. The compatibility conditions are based on interface jump conditions derived from the first order form of Maxwell's equations. For $\rho = 0$, with variable ϵ and μ these are

$$\epsilon(\mathbf{x})\mathbf{E}_t = \nabla \times \mathbf{H}, \qquad \mu(\mathbf{x})\mathbf{H}_t = -\nabla \times \mathbf{E}, \tag{7.1}$$

$$\nabla \cdot (\epsilon(\mathbf{x})\mathbf{E}) = 0, \qquad \nabla \cdot (\mu(\mathbf{x})\mathbf{H}) = 0. \tag{7.2}$$

Under the assumption that $\mathbf{E}$ and $\mathbf{H}$ remain bounded, the basic jump conditions at a material interface $\mathcal{I}$ are derived by integrating each of the equations (7.1-7.2) over an appropriate control volume that spans the interface, (see for example [2]), and the result is

$$[\epsilon \mathbf{n} \cdot \mathbf{E}]_{\mathcal{I}} = 0, \qquad [\mu \mathbf{n} \cdot \mathbf{H}]_{\mathcal{I}} = 0, \tag{7.3}$$

$$[\boldsymbol{\tau}_m \cdot \mathbf{E}]_{\mathcal{I}} = 0, \qquad [\boldsymbol{\tau}_m \cdot \mathbf{H}]_{\mathcal{I}} = 0. \tag{7.4}$$

Here $[\mathbf{f}]_{\mathcal{I}}$ denotes the jump in $\mathbf{f}$ across the interface, $\mathbf{n} = \mathbf{n}(\mathbf{x})$ is the unit normal vector to the interface and $\boldsymbol{\tau}_m = \boldsymbol{\tau}_m(\mathbf{x})$ is a unit tangent vector to the material interface. Since there are two linearly independent tangents in three-dimensions, there will be two linearly independent conditions $[\boldsymbol{\tau}_m \cdot \mathbf{E}] = 0$, $m = 1, 2$ (or just one condition in two-dimensions). Jump conditions on the first spatial derivatives of the solution follow directly from equations (7.2), and also by taking one time derivative of (7.4) and combining with equations (7.1),

$$[\nabla \cdot \mathbf{E}]_{\mathcal{I}} = 0, \qquad [\nabla \cdot \mathbf{H}]_{\mathcal{I}} = 0, \tag{7.5}$$

$$[\mu^{-1}\boldsymbol{\tau}_m \cdot \nabla \times \mathbf{E}]_{\mathcal{I}} = 0, \qquad [\epsilon^{-1}\boldsymbol{\tau}_m \cdot \nabla \times \mathbf{H}]_{\mathcal{I}} = 0. \tag{7.6}$$

Note that $[\nabla \cdot (\epsilon\mathbf{E})]_{\mathcal{I}} = 0$ can be replaced by $[\nabla \cdot \mathbf{E}]_{\mathcal{I}} = 0$ since $\nabla \cdot \mathbf{E}$ is identically zero on either side of the interface. A similar remark applies to the condition $[\nabla \cdot \mathbf{H}]_{\mathcal{I}} = 0$. Additional compatibility conditions can be derived by taking an even number of time derivatives of the four conditions (7.3-7.6) and using the vector wave equation (1.6) to transform the time derivatives into space derivatives. This gives the complete set of interface conditions

$$[\epsilon \mathbf{n} \cdot \Delta^n \mathbf{E}/(\epsilon\mu)^n]_{\mathcal{I}} = 0, \qquad [\mu \mathbf{n} \cdot \Delta^n \mathbf{H}/(\epsilon\mu)^n]_{\mathcal{I}} = 0, \tag{7.7}$$

$$[\boldsymbol{\tau} \cdot \Delta^n \mathbf{E}/(\mu\epsilon)^n]_{\mathcal{I}} = 0, \qquad [\boldsymbol{\tau} \cdot \Delta^n \mathbf{H}/(\mu\epsilon)^n]_{\mathcal{I}} = 0, \tag{7.8}$$

$$[\nabla \cdot (\Delta^n \mathbf{E})]_{\mathcal{I}} = 0, \qquad [\nabla \cdot (\Delta^n \mathbf{H})]_{\mathcal{I}} = 0, \tag{7.9}$$

$$[\mu^{-1}\boldsymbol{\tau} \cdot \nabla \times \Delta^n \mathbf{E}/(\mu\epsilon)^n]_{\mathcal{I}} = 0, \qquad [\epsilon^{-1}\boldsymbol{\tau} \cdot \nabla \times \Delta^n \mathbf{H}/(\mu\epsilon)^n]_{\mathcal{I}} = 0, \tag{7.10}$$

for $n = 0, 1, 2, 3, \ldots$. These interface jump conditions impose constraints on each spatial derivative of the solution.

Discrete versions of the jump conditions are used as numerical boundary conditions in the following manner. First consider the case of a second-order accurate approximation that uses one ghost line on each side of the interface. Let $\mathbf{U}_{\mathbf{i}}^{(k)}$ denote the discrete approximation to the electric field where $k = 1, 2$, denotes the solution on each side of the material interface. The dependence of the solution on time is suppressed for this discussion. To be specific, let the interface correspond to the value of $i_1 = 0$ and the ghost line values correspond to $i_1 = -1$. The values $\mathbf{U}^{(1)}_{-1,i_2,i_3}$ and $\mathbf{U}^{(2)}_{-1,i_2,i_3}$ of the solution on the ghost lines, (one ghost line value on each side of the interface) are determined by imposing the following centered interface conditions at $i_1 = 0$,

$$[\epsilon \mathbf{n} \cdot \Delta_{2h}\mathbf{U}_{\mathbf{i}}^{(k)}/(\epsilon\mu)]_{\mathcal{I}} = 0, \qquad [\boldsymbol{\tau}_m \cdot \Delta_{2h}\mathbf{U}_{\mathbf{i}}^{(k)}/(\mu\epsilon)]_{\mathcal{I}} = 0, \tag{7.11}$$

$$[\nabla_{2h} \cdot (\mathbf{U}_{\mathbf{i}}^{(k)})]_{\mathcal{I}} = 0, \quad [\mu^{-1}\boldsymbol{\tau}_m \cdot \nabla_{2h} \times \mathbf{U}_{\mathbf{i}}^{(k)}]_{\mathcal{I}} = 0. \tag{7.12}$$

Here $\nabla_{2h}\cdot$, $\nabla\times_{2h}$, and Δ_{2h} are some appropriate second-order accurate centered difference approximations. Equations (7.11-7.12) implicitly specify that the time derivatives of the jump conditions (7.3-7.4) are zero (to second-order accuracy). Therefore, by imposing the conditions (7.11-7.12) the basic jump conditions (7.3-7.4) should also be be approximately satisfied (assuming they are satisfied at the initial time). Therefore it may not be essential to explicitly impose the conditions (7.3-7.4). In practice, however, the solution values on the interface itself are constrained to satisfy the basic jump conditions,

$$[\epsilon\mathbf{n}\cdot\mathbf{U}_{\mathbf{i}}^{(k)}]_{\mathcal{I}}=0,\quad [\boldsymbol{\tau}_m\cdot\mathbf{U}_{\mathbf{i}}^{(k)}]_{\mathcal{I}}=0. \tag{7.13}$$

by setting the solution values on the side of the interface with the larger value of ϵ in terms of the values on the other side. For example, if $\epsilon_2\le\epsilon_1$ then

$$\mathbf{U}^{(1)}_{0,i_2,i_3}=\frac{\epsilon_2}{\epsilon_1}(\mathbf{n}\cdot\mathbf{U}^{(2)}_{0,i_2,i_3})\mathbf{n}+\sum_{m=1}^{2}\Big(\boldsymbol{\tau}_m\cdot\mathbf{U}^{(2)}_{0,i_2,i_3}\Big)\boldsymbol{\tau}_m. \tag{7.14}$$

A fourth-order accurate approximation will use two ghost lines on each side of the interface. The values at the ghost points are determined using fourth-order accurate approximations to the interface conditions for the first and second derivatives,

$$[\epsilon\mathbf{n}\cdot\Delta_{4h}\mathbf{U}_{\mathbf{i}}^{(k)}/(\epsilon\mu)]_{\mathcal{I}}=0,\qquad [\boldsymbol{\tau}_m\cdot\Delta_{4h}\mathbf{U}_{\mathbf{i}}^{(k)}/(\mu\epsilon)]_{\mathcal{I}}=0, \tag{7.15}$$

$$[\nabla_{4h}\cdot(\mathbf{U}_{\mathbf{i}}^{(k)})]_{\mathcal{I}}=0,\quad [\mu^{-1}\boldsymbol{\tau}_m\cdot\nabla_{4h}\times\mathbf{U}_{\mathbf{i}}^{(k)}]_{\mathcal{I}}=0, \tag{7.16}$$

together with second-order accurate approximations to the interface conditions for the third and fourth derivatives,

$$[(\nabla\cdot\Delta)_{2h}(\mathbf{U}_{\mathbf{i}}^{(k)})]_{\mathcal{I}}=0,\quad [\mu^{-1}\boldsymbol{\tau}_m\cdot(\nabla\times\Delta)_{2h}\mathbf{U}_{\mathbf{i}}^{(k)}/(\epsilon\mu)]_{\mathcal{I}}=0, \tag{7.17}$$

$$[\epsilon\mathbf{n}\cdot(\Delta^2)_{2h}\mathbf{U}_{\mathbf{i}}^{(k)}/(\epsilon\mu)^2]_{\mathcal{I}}=0,\qquad [\boldsymbol{\tau}_m\cdot(\Delta^2)_{2h}\mathbf{U}_{\mathbf{i}}^{(k)}/(\epsilon\mu)^2]_{\mathcal{I}}=0. \tag{7.18}$$

The fourth-order approximation will also impose equations (7.13). The accuracy and stability of these conditions for a model problem is considered in section 8.

A complicating factor in applying these interface boundary conditions is that the discrete equations couple the unknown values of $\mathbf{U}_{\mathbf{i}}^{(k)}$ at all ghost points on both sides of the interface. Therefore, the solution to these equations requires the solution of a system of equations with number of unknowns proportional to the number of points on the interface. In practice, it has been found that these equations can be approximately solved using an iterative technique (see section 9.3 for further details).

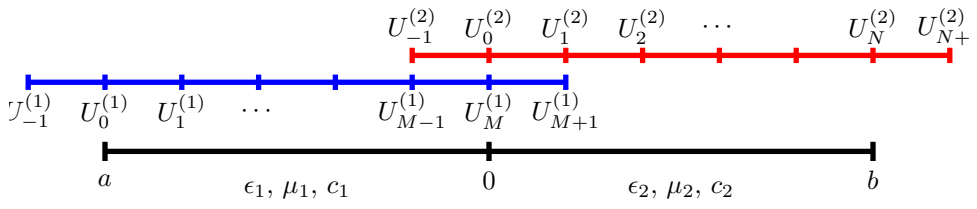

FIG. 4. *The overlapping grids for a one-dimensional material interface located at $x=0$. Ghost points are introduced on the two grids at the interface.*

8. Analysis of the Material Interface Conditions. The accuracy and stability of the centered boundary conditions for material interfaces is considered in this section. A semi-discrete one-dimensional model problem is studied using the Laplace transform in time and mode-analysis in space. Second-order accurate and fourth-order accurate interface conditions are analyzed. A one-dimensional model problem

for $u = u(x,t)$ and $v = v(x,t)$ on the interval $[a,b]$ with a material interface at $x = 0$, $a < x < b$, is

$$\epsilon(x)u_{tt} = u_{xx}, \quad \epsilon(x)v_{tt} = v_{xx}, \tag{8.1}$$

$$[\epsilon u]_{\mathcal{I}} = 0, \qquad [v]_{\mathcal{I}} = 0, \tag{8.2}$$

$$[u_x]_{\mathcal{I}} = 0, \qquad [v_x]_{\mathcal{I}} = 0, \tag{8.3}$$

where $\epsilon(x) = \epsilon_1$ for $x < 0$ and $\epsilon(x) = \epsilon_2$ for $x > 0$. The variable u represents the normal component of the field (say, E_x), while the variable v represents one of the tangential component of the field (say E_y). Note that for this model problem, the equations for the normal and tangential components are decoupled.

Introduce a one-dimensional overlapping grid as shown in Figure 4. A (formally) second-order accurate semi-discrete approximation is

$$\epsilon_1 U_{tt}^{(1)} = D_+D_-U_j^{(1)}, \quad \epsilon_1 V_{tt}^{(1)} = D_+D_-V_j^{(1)}, \quad \text{for } j = M, M-1, M-2\ldots \tag{8.4}$$

$$\epsilon_2 U_{tt}^{(2)} = D_+D_-U_j^{(2)}, \quad \epsilon_2 V_{tt}^{(2)} = D_+D_-V_j^{(2)}, \quad \text{for } j = 0, 1, 2, \ldots \tag{8.5}$$

with interface conditions

$$D_0U_M^{(1)} = D_0U_0^{(2)}, \qquad D_0V_M^{(1)} = D_0V_0^{(2)}, \tag{8.6}$$

$$D_+D_-U_M^{(1)} = D_+D_-U_0^{(2)}, \quad D_+D_-V_M^{(1)}/\epsilon_1 = D_+D_-V_0^{(2)}/\epsilon_2. \tag{8.7}$$

Here $U_i^{(k)}(t)$ and $V_i^{(k)}(t)$ denote the approximations to u and v on the grids while $D_+ = D_{+x}$, $D_- = D_{-x}$, and $D_0 = D_{0x}$ The grid points are denoted by $\mathbf{x}_i^{(k)}$. Approximations to the jump conditions $[u_{xx}]_{\mathcal{I}} = 0$ and $[v_{xx}/\epsilon]_{\mathcal{I}}$ have been imposed in place of (8.2); these follow from equations (8.1-8.2). The interface equations (8.6) and (8.7) can be solved for the values at the ghost points, $U_{M+1}^{(1)}$, $U_{-1}^{(2)}$ in terms of interior values,

$$U_{M+1}^{(1)} = U_1^{(2)} + (U_M^{(1)} - U_0^{(2)}) = U_1^{(2)} + (\epsilon_2/\epsilon_1 - 1)U_0^{(2)} \tag{8.8}$$

$$U_{-1}^{(2)} = U_{M-1}^{(1)} - (U_M^{(1)} - U_0^{(2)}) = U_{M-1}^{(1)} - (1 - \epsilon_1/\epsilon_2)U_M^{(1)} \tag{8.9}$$

$$V_{M+1}^{(1)} = \frac{2\epsilon_1}{\epsilon_1+\epsilon_2}\, V_1^{(2)} + \frac{\epsilon_2-\epsilon_1}{\epsilon_1+\epsilon_2}\big(2V_M^{(1)} - V_{M-1}^{(1)}\big) \tag{8.10}$$

$$V_{-1}^{(2)} = \frac{2\epsilon_2}{\epsilon_1+\epsilon_2}\, V_{M-1}^{(1)} + \frac{\epsilon_1-\epsilon_2}{\epsilon_1+\epsilon_2}\big(2V_0^{(2)} - V_1^{(2)}\big) \tag{8.11}$$

The interface boundary conditions have the useful property that when $\epsilon_1 = \epsilon_2$, the solution to the interface problem is the same as if there were no interface at all.

The stability of the discrete approximations to the interface problem will now be analyzed. A necessary condition for stability is the Godunov-Ryabenkii condition which requires that there be no solutions to following eigenvalue problem for $\mathrm{Re}(s) > 0$,

$$\epsilon_1 s^2 W_j^{(1)} = D_+D_-W_j^{(1)}, \qquad \text{for } j = M, M-1, M-2\ldots, \tag{8.12}$$

$$\epsilon_2 s^2 W_j^{(2)} = D_+D_-W_j^{(2)}, \qquad \text{for } j = 0, 1, 2, \ldots, \tag{8.13}$$

$$D_0W_M^{(1)} = D_0W_0^{(2)}, \qquad (D_+D_-W_M^{(1)})/\epsilon_1^{\alpha} = (D_+D_-W_0^{(2)})/\epsilon_2^{\alpha}, \tag{8.14}$$

$$\|W^{(1)}\|_h < \infty, \qquad \|W^{(2)}\|_h < \infty. \tag{8.15}$$

Here $\alpha = 0$ corresponds to the problem for the normal component $U_i^{(k)}$ while $\alpha = 1$ corresponds to the problem for the tangential component $V_i^{(k)}$. The discrete norms of the grid functions are defined from $\|W^{(1)}\|_h^2 = \sum_{j=-\infty}^{M} |W_j^{(1)}|^2\, h$ and $\|W^{(2)}\|_h^2 = \sum_{j=0}^{\infty} |W_j^{(2)}|^2\, h$. If this problem (8.12-8.15) were to have a solution then there would be a solution to equations (8.4-8.7) of the form $U_i^{(k)}(t) = e^{st}W_i^{(k)}$ that would grow arbitrarily fast in time as $h \to 0$, and the scheme would not be stable.

LEMMA 8.1. *The second-order accurate interface approximation (8.4-8.7) satisfies the Godunov-Ryabenkii condition.*

Proof. The solution to the eigenvalue problem (8.12-8.15) is of the form

$$W_j^{(1)} = A\kappa_1^{M-j}, \quad W_j^{(2)} = B\kappa_2^j,$$

where $\kappa_k = 1 + s_k/2 - \sqrt{s_k}\sqrt{1+s_k/4}$ are roots of the characteristic equation $\kappa - 2 + \kappa^{-1} = s_k$, with $s_k = \epsilon_k s^2 h^2$, for $k = 1, 2$. The branch of the square root is taken so that $|\kappa_1| < 1$ and $|\kappa_2| < 1$ for $\mathrm{Re}(s) > 0$. Applying the interface conditions (8.8) and (8.9) implies

$$\begin{aligned} A(\kappa_1^{-1} - \kappa_1) &= B(\kappa_2 - \kappa_2^{-1}), \\ A(\kappa_1^{-1} - 2 + \kappa_1)/\epsilon_1^\alpha &= B(\kappa_2 - 2 + \kappa_2^{-1})/\epsilon_2^\alpha. \end{aligned}$$

For the case $\alpha = 0$ the determinant condition for nontrivial solutions is

$$(\kappa_1^{-1} - \kappa_1)(\kappa_2 - 2 + \kappa_2^{-1}) = (\kappa_2 - \kappa_2^{-1})(\kappa_1^{-1} - 2 + \kappa_1),$$

which simplifies to $\kappa_1\kappa_2 = 1$. This contradicts the fact that $|\kappa_1\kappa_2| < 1$ and thus there can be no non-trivial solutions. For $\alpha = 1$ it follows that $A = B$ and for a nontrivial solution,

$$-(\kappa_1 - \kappa_1^{-1}) = \kappa_2 - \kappa_2^{-1}.$$

From the definitions of κ_1 and κ_2 it follows that

$$\sqrt{s_1}\sqrt{1+s_1/4} = -\sqrt{s_2}\sqrt{1+s_2/4}.$$

The solution to the last equation is $s_1 = -s_2 - 4$ (the other possible solution $s_1 = s_2$ is on the wrong branch of the square root) which implies

$$s = \pm i/(h\sqrt{\epsilon_1 + \epsilon_2}).$$

This contradicts the assumption that $Re(s) > 0$ and thus there are no nontrivial solutions for $\alpha = 1$. It thus follows that the Godunov-Ryabenkii condition is satisfied □.

The accuracy of the approximation can be determined by examining the problem for the error, $E_i^{(k)} = U_i^{(k)} - u(\mathbf{x}_i^{(k)}, t)$,

$$\begin{aligned} \epsilon_1 s^2 E_j^{(1)} &= D_+D_-E_j^{(1)} + h^2F_1, \qquad \text{for } j = M, M-1, M-2\ldots, \\ \epsilon_2 s^2 E_j^{(2)} &= D_+D_-E_j^{(2)} + h^2F_2, \qquad \text{for } j = 0, 1, 2, \ldots, \\ D_0E_M^{(1)} - D_0E_0^{(2)} &= h^2G_1, \qquad (D_+D_-E_M^{(1)})/\epsilon_1^\alpha - (D_+D_-E_0^{(2)})/\epsilon_2^\alpha = h^2G_2, \end{aligned}$$

where the terms h^2F_1, h^2F_2, h^2G_1 and h^2G_2 are the truncation errors. In the usual manner (for example, see [14]), by subtracting out a solution to the Cauchy problem it may be assumed that $F_1 = F_2 = 0$. The solution to the error equations is then of the form

$$E_j^{(1)} = A\kappa_1^{M-j}, \quad E_j^{(2)} = B\kappa_2^j$$

and applying the interface conditions gives the equations that determine A and B,

$$\begin{bmatrix} (\kappa_1^{-1} - \kappa_1)/(2h) & -(\kappa_2 - \kappa_2^{-1})/(2h) \\ \epsilon_1^{1-\alpha}s^2 & -\epsilon_2^{1-\alpha}s^2 \end{bmatrix} \begin{bmatrix} A \\ B \end{bmatrix} = \begin{bmatrix} h^2G_1 \\ h^2G_2 \end{bmatrix}$$

Using $\kappa_k - \kappa_k^{-1} = -2\sqrt{s_k}\sqrt{1+s_k/4}$, the solution solution for A and B can be determined and is

$$A = \frac{\epsilon_1^{1-\alpha}sG_1 + \epsilon_2^{1/2}G_2}{\epsilon_1^{1-\alpha}(\epsilon_1^{1/2} + \epsilon_2^{1/2})s^2}\ h^2\ + O(h^4), \quad B = \frac{\epsilon_1^{1-\alpha}sG_1 - \epsilon_1^{1/2}G_2}{\epsilon_1^{1-\alpha}(\epsilon_1^{1/2} + \epsilon_2^{1/2})s^2}\ h^2\ + O(h^4).$$

Therefore the solution to the semi-discrete problem is second-order accurate.

Now consider the fourth-order accurate approximation

$$\epsilon_1 U^{(1)}_{tt} = D_+D_-(1-\frac{h^2}{12}D_+D_-)U^{(1)}_j, \quad \text{for } j = M, M-1, M-2\ldots, \tag{8.16}$$

$$\epsilon_2 U^{(2)}_{tt} = D_+D_-(1-\frac{h^2}{12}D_+D_-)U^{(2)}_j, \quad \text{for } j = 0, 1, 2, \ldots, \tag{8.17}$$

$$D_0(1-\frac{h^2}{6}D_+D_-)U^{(1)}_M = D_0(1-\frac{h^2}{6}D_+D_-)U^{(2)}_0, \tag{8.18}$$

$$D_+D_-(1-\frac{h^2}{12}D_+D_-)U^{(1)}_M/\epsilon_1^\alpha = D_+D_-(1-\frac{h^2}{12}D_+D_-)U^{(2)}_0/\epsilon_2^\alpha, \tag{8.19}$$

$$D_0D_+D_-U^{(1)}_M/\epsilon_1 = D_0D_+D_-U^{(2)}_0/\epsilon_2, \tag{8.20}$$

$$(D_+D_-)^2U^{(1)}_M/\epsilon_1^{1+\alpha} = 0(D_+D_-)^2U^{(2)}_0/\epsilon_2^{1+\alpha}. \tag{8.21}$$

where $\alpha = 0$ corresponds to the interface conditions for the normal component and $\alpha = 1$ the conditions for the tangential component. Two ghost points have been added to the grids on each side of the interface. Appropriate initial conditions are also required to complete the specification of the problem; their precise form is not germane to the following discussion. When $\epsilon_1 = \epsilon_2$, the solution to the interface problem reduces to the solution of the equations with no interface present since in this case $U^{(1)}_{M+m} = U^{(2)}_m$ and $U^{(2)}_{-m} = U^{(1)}_{M+m}$ for $m = 1, 2$.

The Godunov-Ryabenkii condition, necessary for the stability of solutions to these difference equations, requires that there be no solutions with $\mathrm{Re}(s) > 0$ to the eigenvalue problem

$$\begin{aligned}
\epsilon_1 s^2 W^{(1)}_j &= D_+D_-(1-\frac{h^2}{12}D_+D_-)W^{(1)}_j, \quad \text{for } j = M, M-1, M-2\ldots,\\
\epsilon_2 s^2 W^{(2)}_j &= D_+D_-(1-\frac{h^2}{12}D_+D_-)W^{(2)}_j, \quad \text{for } j = 0, 1, 2, \ldots,\\
D_0(1-\frac{h^2}{6}D_+D_-)W^{(1)}_M &= D_0(1-\frac{h^2}{6}D_+D_-)W^{(2)}_0,\\
D_+D_-(1-\frac{h^2}{12}D_+D_-)W^{(1)}_M/\epsilon_1^\alpha &= D_+D_-(1-\frac{h^2}{12}D_+D_-)W^{(2)}_0/\epsilon_2^\alpha,\\
D_0D_+D_-W^{(1)}_M/\epsilon_1 &= D_0D_+D_-W^{(2)}_0/\epsilon_2,\\
(D_+D_-)^2W^{(1)}_M/\epsilon_1^{1+\alpha} &= 0(D_+D_-)^2W^{(2)}_0/\epsilon_2^{1+\alpha},\\
\|W^{(1)}\|_h < \infty, &\qquad \|W^{(2)}\|_h < \infty.
\end{aligned}$$

LEMMA 8.2. *The fourth-order accurate interface approximation (8.16-8.21) satisfies the Godunov-Ryabenkii condition for* $sh \ll 1$.

Proof. For $\mathrm{Re}(s) > 0$ the bounded solutions may be written as

$$W^{(1)}_j = A_1\kappa_1^{M-j} + B_1\widetilde{\kappa}_1^{M-j}, \quad W^{(2)}_j = A_2\kappa_2^{j} + B_2\widetilde{\kappa}_2^{j},$$

where κ_k are the roots approximating the solution to the continuous problem and $\widetilde{\kappa}_k$ are the spurious roots. These are roots of the characteristic equation

$$s_k = (\kappa - 2 + \kappa^{-1})(1 - \frac{1}{12}(\kappa - 2 + \kappa^{-1})) = s_k,$$

where $s_k = \epsilon_k s^2 h^2$. In particular

$$\begin{aligned}
\kappa_k &= 1 + z_k/2 - \sqrt{z_k}\sqrt{1 + z_k/4}, \quad & \widetilde{\kappa}_k &= 1 + \widetilde{z}_k/2 - \sqrt{\widetilde{z}_k}\sqrt{1 + \widetilde{z}_k/4},\\
z_k &= 6(1 - \sqrt{1 - s_k/3}), & \widetilde{z}_k &= 6(1 + \sqrt{1 - s_k/3}),
\end{aligned}$$

where the branch of the square root is chosen so that $|\kappa_k| < 1$ and $|\widetilde{\kappa}_k| < 1$ for $Re(s) > 0$. For $sh \ll 1$, these roots take the form

$$\kappa_k = 1 - \sqrt{\epsilon_k} sh + \epsilon_k (sh)^2/2 - (\sqrt{\epsilon_k} sh)^3/6 + (\sqrt{\epsilon_k} sh)^4/24 + O((sh)^5),$$
$$\widetilde{\kappa}_k = \frac{1}{7+4\sqrt{3}} + O(sh).$$

It can be seen that κ_k is a fourth-order approximation to $e^{-\sqrt{\epsilon_k} sh}$. Substitution of $W_j^{(1)}$ and $W_j^{(1)}$ into the four boundary conditions implies

$$\begin{bmatrix} \mathcal{D}_1(\kappa_1) & \mathcal{D}_1(\widetilde{\kappa}_1) & \mathcal{D}_1(\kappa_2) & \mathcal{D}_1(\widetilde{\kappa}_2) \\ s_1/\epsilon_1^\alpha & s_1/\epsilon_1^\alpha & -s_2/\epsilon_2^\alpha & -s_2/\epsilon_2^\alpha \\ \mathcal{D}_3(\kappa_1)/\epsilon_1 & \mathcal{D}_3(\widetilde{\kappa}_1)/\epsilon_1 & \mathcal{D}_3(\kappa_2)/\epsilon_2 & \mathcal{D}_3(\widetilde{\kappa}_2)/\epsilon_2 \\ \mathcal{D}_4(\kappa_1)/\epsilon_1^{1+\alpha} & \mathcal{D}_4(\widetilde{\kappa}_1)/\epsilon_1^{1+\alpha} & -\mathcal{D}_4(\kappa_2)/\epsilon_2^{1+\alpha} & -\mathcal{D}_4(\widetilde{\kappa}_2)/\epsilon_2^{1+\alpha} \end{bmatrix} \begin{bmatrix} A_1 \\ B_1 \\ A_2 \\ B_2 \end{bmatrix} = \mathbf{0} \tag{8.22}$$

where $\mathcal{D}_1(\kappa) = \frac{1}{2}(\kappa - \kappa^{-1})(1 - \frac{1}{6}(\kappa - 2 + \kappa^{-1}))$, $\mathcal{D}_3(\kappa) = \frac{1}{2}(\kappa - \kappa^{-1})(\kappa - 2 + \kappa^{-1})$, and $\mathcal{D}_4(\kappa) = (\kappa - 2 + \kappa^{-1})^2$. Let $\mathcal{M}$ denote the matrix appearing in equation (8.22). Note that $\kappa_k - \kappa_k^{-1} = -2\sqrt{z_k}\sqrt{1 + z_k/4}$ and $\kappa_k - 2 + \kappa_k^{-1} = z_k$ which can be used to simplify the entries in $\mathcal{M}$. For stability there should be no values of s with $Re(s) > 0$ when the determinant of $\mathcal{M}$ is zero. This condition is difficult to prove for general values of sh. For $sh \ll 1$, corresponding to the resolved modes in the discrete solution, the elements of the determinant can be expanded in powers of sh and one finds that for $sh \to 0$,

$$\det(\mathcal{M}) \sim -2^9 3^3 \sqrt{3}(\epsilon_1^{-1/2} + \epsilon_2^{-1/2})\ (sh)^3, \qquad \text{for } \alpha = 0, \tag{8.23}$$

$$\det(\mathcal{M}) \sim -2^8 3^3 \sqrt{3} \frac{1}{\epsilon_1^2 \epsilon_2^2}(\epsilon_1^{1/2} + \epsilon_2^{1/2})(\epsilon_1 + \epsilon_2)\ (sh)^3, \quad \text{for } \alpha = 1. \tag{8.24}$$

Therefore there are no unstable modes for $sh \ll 1$ with $Re(s) > 0$. This proves the lemma □.

To gain some confidence that there are no unstable modes for larger values of sh one can graph the surface $\mathcal{S}(sh) = |\det(\mathcal{M}(sh))|$ as a function of the complex number sh and look for places where $\mathcal{S}(sh) = 0$ for $Re(sh) > 0$. Figure 5 shows a plot of $\mathcal{S}(sh)$ for $\epsilon_1 = 1$, $\epsilon_2 = 16$, and for $\alpha = 0, 1$. The figure also shows plots of $\mathcal{S}(sh)$, along the line $Im(sh) = 0$, compared to the asymptotic forms (8.23-8.24). The asymptotic forms agree with the computed values of the determinant. Although the surface $\mathcal{S}(sh)$ has a local minimum for $.4 < Re(sh) < .5$, the values are still far from zero. These graphical results support the conjecture that the determinant of $\mathcal{M}$ is never zero for $Re(s) > 0$; it is therefore likely that the fourth-order discrete scheme always satisfies the Godunov-Ryabenkii condition, at least for the values of ϵ_1 and ϵ_2 that have been investigated.

9. Implementation of the scheme. Some aspects of the implementation of the discrete approximations to the differential operators and boundary conditions will be considered in this section. The intent of these remarks is to give a basic outline of the implementation, a more detailed description is left for a future report. In typical cases the majority of grid points on an overlapping grid belong to Cartesian grids where the discrete approximations are straight-forward to implement. The Cartesian grid approximations are very fast to evaluate and use little memory. The majority of the programming effort, however, is concerned with implementing the approximations to the boundary conditions and material interface conditions on curvilinear grids.

9.1. Solving the PEC boundary conditions. The solution of the discrete approximations to the boundary conditions for a perfect electrical conductor are based upon the boundary conditions $\mathbf{n} \times \mathbf{E} = 0$ and $\nabla \cdot \mathbf{E} = 0$, together with the compatibility conditions (3.4). In order to simplify the implementation, some approximations are made that do not seem to affect the overall accuracy, as evidenced by the numerical results from section 10. In general curvilinear coordinates the divergence of $\mathbf{E}$ can be

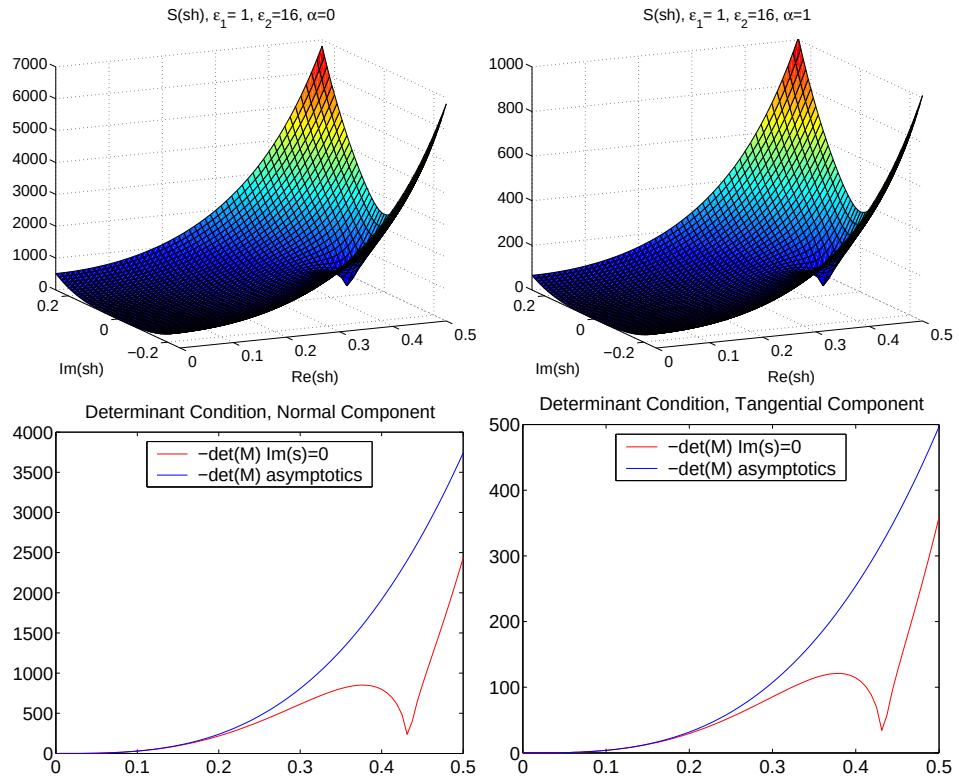

FIG. 5. *Top: a plot of the surface* $\mathcal{S}(sh) = |\det(\mathcal{M}(sh))|$ *for the fourth-order accurate discrete interface problem with* $\epsilon_1 = 1$, $\epsilon_2 = 16$ *and* $\alpha = 0$ *(left) and* $\alpha = 1$ *(right). Stability of the discrete approximation requires that* $\mathcal{S} > 0$ *for* $Re(sh) > 0$. *Bottom: A comparison of* $\mathcal{S}$ *to the asymptotic forms (8.23-8.24) along the line* $Im(sh) = 0$ *for* $\alpha = 0$ *(left) and* $\alpha = 1$ *(right).*

written as

$$\nabla \cdot \mathbf{E} = \frac{1}{J} \sum_{m=1}^{d} \frac{\partial}{\partial r_m} (\mathbf{a}_m \cdot \mathbf{E}),$$
$$\mathbf{a}_m = J \nabla_{\mathbf{x}} r_m \ = J(\partial_x r_m, \partial_y r_m, \partial_z r_m) \ .$$

For a PEC boundary, corresponding to the parameter space line $r_1 = 0$, the boundary condition $\nabla \cdot \mathbf{E} = 0$ becomes a condition relating the r_1-derivative of $\mathbf{a}_1 \cdot \mathbf{E} = -J \|\nabla_{\mathbf{x}} r_1\| \mathbf{n} \cdot \mathbf{E}$ to tangential derivatives of the components $\mathbf{a}_2 \cdot \mathbf{E}_2$ and $\mathbf{a}_3 \cdot \mathbf{E}$,

$$\partial_{r_1}(\mathbf{a}_1 \cdot \mathbf{E}) = -\partial_{r_2}(\mathbf{a}_2 \cdot \mathbf{E}_2) - \partial_{r_3}(\mathbf{a}_3 \cdot \mathbf{E}) \ .$$

For an orthogonal grid, $\mathbf{a}_2 \cdot \mathbf{E}(0, r_2, r_3) = 0$ and $\mathbf{a}_3 \cdot \mathbf{E}(0, r_2, r_3) = 0$ on the boundary since $\mathbf{a}_2$ and $\mathbf{a}_3$ are in the tangent plane. In addition, $\mathbf{a}_1 \cdot \mathbf{E}$ is (always) proportional to the normal component of $\mathbf{E}$, and thus the $\nabla \cdot \mathbf{E} = 0$ boundary condition reduces to a normal derivative of this component

$$\nabla \cdot \mathbf{E} = \partial_{r_1}(\mathbf{a}_1 \cdot \mathbf{E}), \quad \text{for } r_1 = 0 \quad \text{(orthogonal grid)}.$$

For general grids $\mathbf{a}_2 \cdot \mathbf{E}_2$ and $\mathbf{a}_3 \cdot \mathbf{E}$ are not zero. A second-order accurate approximation to the boundary conditions at $i_1 = 0$ is

$$\boldsymbol{\tau}_m \cdot \mathbf{U_i} = 0, \tag{9.1}$$
$$D_{0,r_1}(\mathbf{a}_1 \cdot \mathbf{U_i}) = -D_{0,r_2}(\mathbf{a}_2 \cdot \mathbf{U_i}) - D_{0,r_3}(\mathbf{a}_3 \cdot \mathbf{U_i}), \tag{9.2}$$
$$\boldsymbol{\tau}_m \cdot D_{+r} D_{-r} \mathbf{U_i} = 0, . \tag{9.3}$$

where $\boldsymbol{\tau}_m$, $m = 1, 2$ are tangent vectors to the boundary (there is only one in two-dimensions). The equations (9.2-9.3) determine the solution on the ghost point,

$\mathbf{U}_{-1,i_2,i_3}$. Equation (9.3) approximates the more accurate compatibility condition $\boldsymbol{\tau}_m \cdot \Delta\mathbf{E} = 0$. These equations can be solved without iteration since the terms appearing on the right hand side of equation (9.2) involve known values on the boundary once equation (9.1) is applied.

Let $D^{(4)}_{r_m} = D_{0,r_m}(1 - \frac{1}{12}\Delta {r_1}^2 D_{+,r_m} D_{-,r_m})$ denote the fourth-order accurate approximation to $\partial/\partial r_m$. A fourth-order accurate approximation to the boundary conditions at $i_1 = 0$ is

$$\boldsymbol{\tau}_m \cdot \mathbf{U}_\mathbf{i} = 0, \tag{9.4}$$

$$D^{(4)}_{r_1}(\mathbf{a}_1 \cdot \mathbf{U})_\mathbf{i} = -D^{(4)}_{r_2}(\mathbf{a}_2 \cdot \mathbf{U}_\mathbf{i}) - D^{(4)}_{r_3}(\mathbf{a}_3 \cdot \mathbf{U}_\mathbf{i}), \tag{9.5}$$

$$\boldsymbol{\tau}_m \cdot (\Delta_{4h}\mathbf{U}_\mathbf{i}) = 0, \tag{9.6}$$

$$D_{0,r_1}(\mathbf{a}_1 \cdot \Delta_{2h}\mathbf{U}_\mathbf{i}) = 0, \tag{9.7}$$

$$(D_{+,r_1}D_{-,r_1})^2(\boldsymbol{\tau}_m \cdot \mathbf{U}_\mathbf{i}) = 0. \tag{9.8}$$

Equations (9.5-9.7) will determine the solution at the two ghost lines, $\mathbf{U}_{-1,i_2,i_3}$ and $\mathbf{U}_{-2,i_2,i_3}$. Condition (9.8) is an approximation to the more accurate compatibility condition $\Delta^2_{2h}(\boldsymbol{\tau}_m \cdot \mathbf{U}_\mathbf{i}) = 0$. Δ_{4h} is the fourth-order accurate FD4 approximation, and Δ_{2h} is the second-order accurate FD2 approximation to the Laplacian as defined in section 5. Equations (9.6-9.7) couple the unknown values at the ghost points with neighbouring points. These equations can be solved by iterating on the unknown values using an appropriate initial guess, only one or two iterations are normally required.

9.2. Numerical dissipation. A high-order dissipation is added to the scheme to stabilize the approximation from weak, high-frequency, instabilities that may develop near interpolation points and boundaries. At the continuous level the dissipation of the second-order wave equation takes the form $u_{tt} = c^2\Delta u - \alpha\ h^{2p}(-\Delta)^p u_t$, where h is a measure of the local grid spacing. For the fourth-order accurate scheme a fourth-order dissipation with $p = 2$ is typically used,

$$\begin{aligned} U^{n+1}_\mathbf{i} - 2U^n_\mathbf{i} + U^{n-1}_\mathbf{i} &= (c\Delta t)^2\Delta_{4h}U_\mathbf{i} + \frac{(c\Delta t)^4}{12}(\Delta^2)_{2h}U_\mathbf{i} \\ &\quad - \alpha_d(c\Delta t)^2 \sum_{m=1}^{d} (\Delta r_m)^4 (D_{+r_m}D_{-r_m})^2 (U^n_\mathbf{i} - U^{n-1}_\mathbf{i})/\Delta t. \end{aligned} \tag{9.9}$$

The coefficient α_d is typically chosen to be about 1. The scheme remains fourth-order accurate provided $\alpha_d = O(1)$. It is also possible to use a sixth-order dissipation with the fourth order scheme, but this does not seem to provide any significant advantage.

9.3. Material interfaces. The boundary conditions for material interfaces have been implemented in two-dimensions. Both second- and fourth-order approximations have been developed, see section 10.5 for a sample fourth-order accurate computation. The implementation is currently restricted to the case when the grids that meet at the interface have matching grids points (as shown, for example, in the grid in Figure 10).

The solution of the fourth-order accurate approximations in two-dimensions will be discussed here, the second-order accurate case is similar. Assume, as in section 7, that the interface corresponds to the line $i_1 = 0$, with the unknown ghost point values being $\mathbf{U}^{(k)}_{-m,i_2,i_3}$, for the ghost lines $m = 1, 2$, on the two sides of the interface, $k = 1, 2$. As a first step, the basic jump conditions (7.3–7.4) for the electric field are imposed. These conditions are used to assign the values of the electric field $\mathbf{U}^{(k)}_{0,i_2,i_3}$ for the side of the interface with the larger value of ϵ. The interface compatibility conditions are given by equations (7.15–7.18). The solution to these equations will determine the values at the ghost points on both sides of the interface. Approximations for Δ_{4h}, ∇_{4h} $(\nabla \cdot \Delta)_{2h}$ etc. are obtained with the mapping method (section 5). Three of the conditions (7.15,7.17,7.18) cause the equations to be coupled between adjacent points along the boundary, although on an orthogonal grid only the higher-order correction conditions (7.17,7.18) lead to coupling. At the start of the iteration the values on the

ghost points on both sides of the interface are given initial values by extrapolation. Then, at each step in the iteration, a small system of equations is solved at each point, $(0, i_2)$ along the boundary, for the 8 unknown values $\mathbf{U}^{(k)}_{-m,i_2,i_3}$, $m = 1, 2$, $k = 1, 2$ using the 8 equations (7.15–7.18). There will be 12 unknowns and 12 equations in three-dimensions. When solving these equations the values at adjacent points are kept fixed at their most recent values. In practice it seems that one or two iterations is sufficient to solve these interface equations.

9.4. Parallel implementation. The algorithms described here have been implemented in the computer code **mx**. The **mx** solver is implemented at a high level in C++. It is based upon the Overture class library [38]. Most of the numerically intensive kernels are written in Fortran77. The overhead in using C++ is found to be negligible for any reasonable size problem (see section 10.6). The computer code **mx** runs on both serial and distributed memory parallel computers.

In a distributed parallel computing environment, the grid functions on each component grid (representing the solution variables such as E_x, E_y, E_z, etc.) are represented as multi-dimensional arrays. These arrays can be distributed across one or more processors. The grid functions are implemented using parallel distributed arrays from the P++ array class library [30]. Each P++ array can be independently distributed across the available processors. The distributed array consists of a set of serial arrays, one serial array for each processor. Each serial array is a multi-dimensional array that can be operated on using array operations. The data from the serial array can also be passed to a Fortran function, for example. When running in parallel, the serial arrays contain extra ghost lines that hold copies of the data from the serial arrays on neighbouring processors. P++ is built on top of the Multiblock PARTI parallel communication library [36], which is used for ghost boundary updates and copying blocks of data between arrays with possibly different parallel distributions.

A special parallel overlapping grid interpolation routine has been developed for updating the points on grids that interpolate from other grids (the interpolation points are shown, for example, in Figure 1). Overlapping grid interpolation is based on a multi-dimensional tensor product Lagrange interpolant, defined in section 4. In parallel, the Lagrange formula is evaluated on the processor that owns the data in the stencil (the donor points), the resulting sums are collected into a message and then sent to the processor that owns the interpolation points. There is at most one message that needs to be sent between any two processors. In this way, the number of messages and the size of the messages that need to be passed between processors is quite small.

Figure 6 shows some results from solving Maxwell's equations with the **mx** solver on a distributed memory Linux cluster (with 2.4 Ghtz Zeon processors). The equations are solved to fourth-order accuracy. In these examples the number of grid points remains fixed as the number of processors is increased. The figure compares two-dimensional results for a square with 1024^2 ($1.1e6$) grid points to that of a circle-in-channel overlapping grid with $3.8e6$ grid points. The parallel scaling is very good in two-dimensions for these problems since the number of computational points is large compared to the number of points where communication is required. Also shown are three-dimensional results for a box with 256^3 ($1.78e7$) grid points compared to a grid for a pill-box with about $3.2e6$ grid points (the pill-box appears in Figure 11). In the three-dimensional cases, there are relatively many more points where communication is required since for N^3 grid points in three-dimensions there are $O(N^2)$ points on the inter-processor boundaries. The parallel scaling is still reasonable with the results for the overlapping grid being comparable to that for the box.

10. Numerical results.

10.1. The method of analytic solutions. The *method of analytic solutions* is an extremely useful technique for constructing exact solutions to check the accuracy of a computer program. This method, also sometimes known as the *method of manufactured solutions* [32], or *twilight-zone forcing* [5] adds forcing functions to

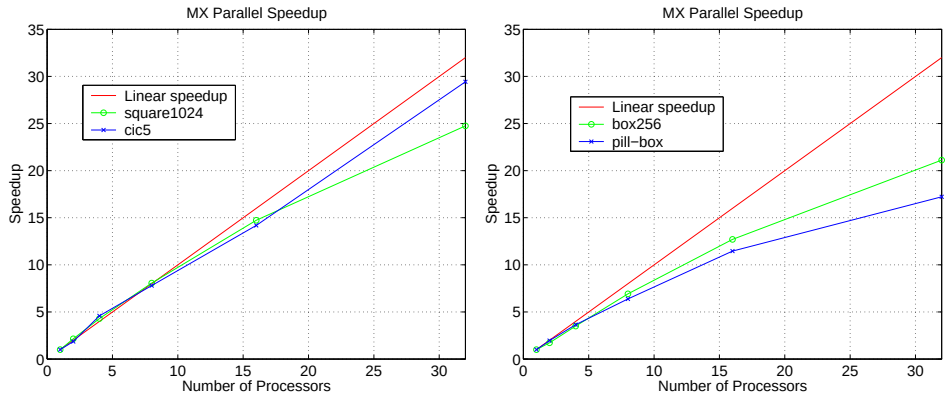

FIG. 6. *Parallel results for the fourth-order accurate Maxwell solver. Left: speedup for a square with* 1024^2 *(1.1e6) points compared to a two-dimensional circle-in-a-channel grid with* 3.8e6 *grid points. Right: speedup for a box with* 256^3 *(1.78e7) grid points, compared to a pill-box grid with* 3.2e6 *grid points. Computations were performed on a Linux cluster.*

the governing equations and boundary conditions. These forcing functions are determined so that some given functions, $\mathbf{E}^{\rm true}(\mathbf{x},t)$, will be the exact solution to the forced equations. With this approach, the error in the discrete solution can be easily determined. Two common choices for exact solutions are low degree polynomials or trigonometric functions. The polynomial solutions are useful for checking that the fourth-order scheme can exactly solve a problem on a Cartesian grid when the degree of the polynomials is less than or equal to four. The trigonometric functions will be used in the convergence results given in this section. The exact solutions are chosen to be divergence free. In two- and three-dimensions the functions are

$$(E_x^{\rm true},E_y^{\rm true},H_z^{\rm true}) = \Big(\frac{1}{2}c_xc_y,\frac{1}{2}s_xs_y,c_xs_y\Big)\cos(\pi t),$$
$$(E_x^{\rm true},E_y^{\rm true},E_z^{\rm true}) = \Big(c_xc_yc_z,\frac{1}{2}s_xs_yc_z,\frac{1}{2}s_xc_ys_z\Big)\cos(\pi t),$$

where $c_x=\cos(\pi x)$, $s_y=\sin(\pi x)$, etc. Define the error in the discrete approximation $U_{\mathbf{i}}^n$ to E_x at a given time t^n by

$$\mathrm{e}_{\mathbf{i}}^{E_x} = U_{\mathbf{i}}^n - E_x^{\rm true}(\mathbf{x}_{\mathbf{i}},t^n)\ , \tag{10.1}$$

with similar definitions for $\mathrm{e}_{\mathbf{i}}^{E_y}$, $\mathrm{e}_{\mathbf{i}}^{E_z}$ and $\mathrm{e}_{\mathbf{i}}^{H_z}$ Define the discrete max-norm by

$$\|U_{\mathbf{i}}^n\|_\infty = \max_{\mathbf{i}}|U_{\mathbf{i}}^n|\ , \tag{10.2}$$

where the maximum is taken over all valid points in the overlapping grid.

Table (2) shows convergence results for a two-dimensional cylinder in a channel. The coarse grid, $\mathcal{G}_1$, for this case consists of a Cartesian grid for the square $[-2,2]^2$ with 61×61 grid points, and an annular grid centered at the origin with inner radius $\frac{1}{2}$, outer radius $\frac{3}{4}$ and containing 81×5 grid points. The grids $\mathcal{G}_2$ and $\mathcal{G}_4$ are, respectively, two and four times finer in each direction. PEC boundary conditions are taken on all boundaries. The results in the table show that the solution is converging at a rate close to 4 in the maximum norm. The non-dimensionalized divergence in $\mathbf{E}$, defined as $\delta_{\mathbf{E}} = \|\nabla\cdot\mathbf{E}\|_\infty/\|\nabla\mathbf{E}\|_\infty$, is small and also converging at a rate close to 4. The convergence rate σ was estimated by assuming an error of the form $E=Ch^\sigma$ and making a least squares fit for σ to the equation $\log(E)=\sigma\ \log(h)+\log(C)$.

Table (2) shows convergence results for solutions computed on a sphere in a box domain. The coarse grid, $\mathcal{G}_1$, in this case consists of three grids. A Cartesian grid covers the cube $[-2,2]^3$ with 41^3 grid points. The sphere of radius $\frac{1}{2}$ is covered with two overlapping orthographic patches, each with $33\times33\times13$ grid points. The grids $\mathcal{G}_2$ and $\mathcal{G}_4$ are, respectively, two and four times finer in each direction. The fine

grid	$\|e^{E_x}\|_\infty$	$\|e^{E_y}\|_\infty$	$\|e^{H_z}\|_\infty$	$\delta_{\mathbf{E}}$
$\mathcal{G}_1$	$9.1e{-5}$	$6.4e{-5}$	$1.3e{-4}$	$1.7e{-4}$
$\mathcal{G}_2$	$4.2e{-6}$	$4.5e{-6}$	$8.1e{-6}$	$1.1e{-5}$
$\mathcal{G}_4$	$2.2e{-7}$	$2.9e{-7}$	$5.1e{-7}$	$7.8e{-7}$
rate σ	4.40	3.93	4.02	3.94

TABLE 1

Convergence rates for a two-dimensional cylinder in a channel grid. The maximum errors in E_x, E_y, H_z and $\delta_{\mathbf{E}} = \|\nabla \cdot \mathbf{E}\|_\infty / \|\nabla \mathbf{E}\|_\infty$ are shown at $t = 1$. for a trigonometric exact solution. The estimated convergence rate, $E \propto h^\sigma$, is also indicated.

grid $\mathcal{G}_4$ has about 6.4 million grid points. PEC boundary conditions are taken on all boundaries. The results in the table show the maximum errors and estimated convergence rates. The convergence rates for the errors in $\mathbf{E}$ are close to 4. The convergence rate for $\delta_{\mathbf{E}}$ is approximately 3.5 which is still reasonable considering that this quantity is derived from derivatives of the computed variables.

grid	$\|e^{E_x}\|_\infty$	$\|e^{E_y}\|_\infty$	$\|e^{E_z}\|_\infty$	$\delta_{\mathbf{E}}$
$\mathcal{G}_1$	$1.1e{-3}$	$6.0e{-4}$	$1.4e{-3}$	$3.0e{-3}$
$\mathcal{G}_2$	$4.8e{-5}$	$1.9e{-5}$	$6.0e{-5}$	$2.1e{-4}$
$\mathcal{G}_4$	$3.7e{-6}$	$1.6e{-6}$	$4.6e{-6}$	$2.4e{-5}$
rate σ	4.12	4.26	4.11	3.47

TABLE 2

Convergence rates for a three dimensional sphere in a box domain. The maximum errors in E_x, E_y, E_z and the non-dimensionalized divergence $\delta_{\mathbf{E}}$ are shown at $t = 1$. for a trigonometric exact solution. The estimated convergence rate, $E \propto h^\sigma$, is also indicated.

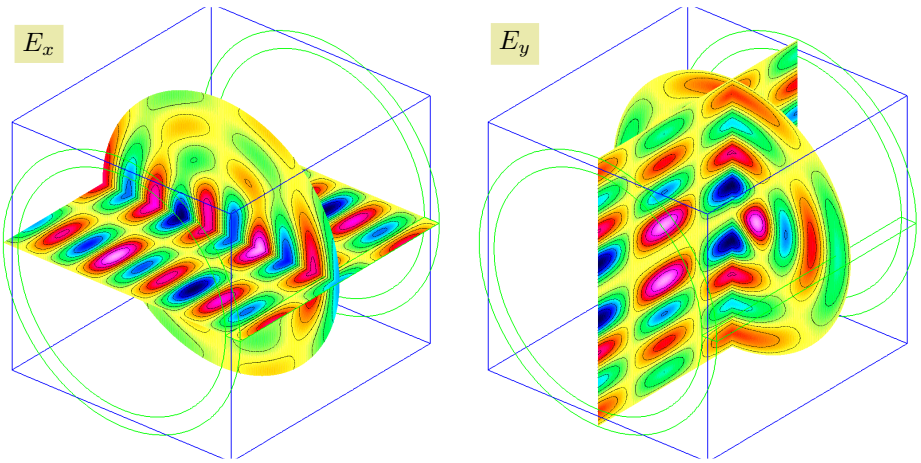

FIG. 7. *The computed solution for the eigenmode $(n, p, k) = (2, 3, 3)$ of a cylindrical cavity at $t = 1$. The electric field components E_x and E_y are shown. The block boundaries of the component grids are also shown.*

10.2. Eigenfunctions of a cylindrical cavity. The eigenfunctions of Maxwell's equations for a three-dimensional cylindrical cavity can be used to test the accuracy of the numerical scheme. Consider a cylindrical cavity, $\mathcal{C}(d)$ of length d, and radius

1, $\mathcal{C}(d) = \{\mathbf{x} \mid x_1^2 + x_2^2 < 1\ ,\ 0 < x_3 < d\}$. The eigenfunctions of the domain $\mathcal{C}(d)$ are

$$
\begin{aligned}
E^x_{p,n,k}(r,\theta,z,t) &= -\frac{(k\pi/d)}{\lambda^2_{p,n}}\big\{A_{p,n}\cos(\theta) + B_{p,n}\sin(\theta)\big\}\sin(k\pi z/d)\cos(\omega_{p,n}t),\\
E^y_{p,n,k}(r,\theta,z,t) &= -\frac{(k\pi/d)}{\lambda^2_{p,n}}\big\{A_{p,n}\sin(\theta) - B_{p,n}\cos(\theta)\big\}\sin(k\pi z/d)\cos(\omega_{p,n}t),\\
E^z_{p,n,k}(r,\theta,z,t) &= J_n(\lambda_{p,n}r)\cos(n\theta)\cos(k\pi z/d)\cos(\omega_{p,n}t),\\
A_{p,n} &= \lambda_{p,n}J_n'(\lambda_{p,n}r)\cos(n\theta), \quad B_{p,n} = \frac{n}{r}J_n(\lambda_{p,n}r)\sin(n\theta),\\
n &= 0,1,2,3,\ldots, \quad p = 1,2,3,\ldots, \quad k = 1,2,3,\ldots
\end{aligned}
$$

where $\lambda_{p,n}$ are the zeros of the Bessel function, $J_n(\lambda_{p,n}) = 0$, and the values of frequencies in time are $\omega_{p,n,k} = \sqrt{(\frac{k\pi}{d})^2 + \lambda^2_{p,n}}$.

grid	$\|\mathrm{e}^{E_x}\|_\infty$	$\|\mathrm{e}^{E_y}\|_\infty$	$\|\mathrm{e}^{E_z}\|_\infty$	$\delta_{\mathbf{E}}$
$\mathcal{G}_1$	$2.5e{-}2$	$2.5e{-}2$	$1.2e{-}1$	$1.1e{-}1$
$\mathcal{G}_2$	$1.4e{-}3$	$1.4e{-}3$	$7.5e{-}3$	$4.2e{-}3$
$\mathcal{G}_4$	$1.1e{-}4$	$1.1e{-}4$	$5.1e{-}4$	$4.9e{-}4$
$\mathcal{G}_8$	$7.4e{-}6$	$7.4e{-}6$	$3.3e{-}5$	$3.5e{-}5$
rate σ	3.89	3.89	3.94	3.78

TABLE 3

Maximum errors at $t = 1$ and estimated convergence rate in computing eigen-mode $(2,3,3)$ of a three-dimensional cylindrical cavity.

The three-dimensional vector wave equation for $\mathbf{E}$ is solved in the cylindrical cavity. The coarse grid, $\mathcal{G}_1$, for this region consists of a cylindrical shell of inner radius $\frac{4}{10}$ and outer radius 1 with 7 points in the radial direction, 53 points in the circumferential direction, and 21 points in the axial direction. The refined grids $\mathcal{G}_2$, $\mathcal{G}_4$ and $\mathcal{G}_8$ increase the grid resolution by a factor of 2 in each case. The radial width of the cylindrical grid is reduced as the mesh spacing is refined so that the number of points in the radial direction on the cylindrical grid is nearly constant. All boundaries are taken as PEC boundaries. The initial conditions are taken to be the exact solution at times $t = 0$ and $t = -\Delta t$. The solution is integrated to time $t = 1$. Table 3 present convergence results for computing the eigenfunction with $(n,p,k) = (2,3,3)$. The maximum errors in the solution and the maximum value of $\delta_{\mathbf{E}}$ are given. The estimated convergence rates are close to 4, as to be expected for the fourth-order approximation. Figure 7 shows the computed solution at time $t = 1$ for this mode $(n,p,k) = (2,3,3)$.

10.3. Scattering by a PEC cylinder. The scattering of a plane wave by a two-dimensional metallic cylinder of radius a is considered. For an incident field

$$
\mathbf{E}^I_x = 0\ , \quad \mathbf{E}^I_y = -\sqrt{\frac{\mu}{\epsilon}}\ e^{i(kx-\omega t)}, \quad H^I_z = \hat{z}e^{i(kx-\omega t)},
$$

the scattered field for H_z (from which the electric field can be easily determined) is given by $H^S_z(\mathbf{x},t) = Re(\mathcal{H}^S(\mathbf{x},\omega)e^{-i\omega t})$ where the complex valued $\mathcal{H}^S$ is given by [39],

$$
\mathcal{H}^S = -\sum_{n=0}^{\infty}\epsilon_n i^n \frac{J_n'(ka)}{H_n^{(1)'}(ka)}H_n^{(1)}(kr)\cos(n\theta)\ .
$$

Here (r,θ) are the usual polar coordinates variables, J_n and Y_n are the Bessel functions of first and second kind, $H_n^{(1)}(z) = J_n + iY_n$ is the Hankel function of the first kind and $\epsilon_0 = 1$, $\epsilon_n = 2$, $n = 1,2,\ldots$. The known incident field can be subtracted out, leaving the solution to the scattered field, $\mathbf{E}^S$ and H^S_z, to be determined. The initial conditions for $t = -\Delta t$ and $t = 0$ are taken as the exact solution for the scattered field.

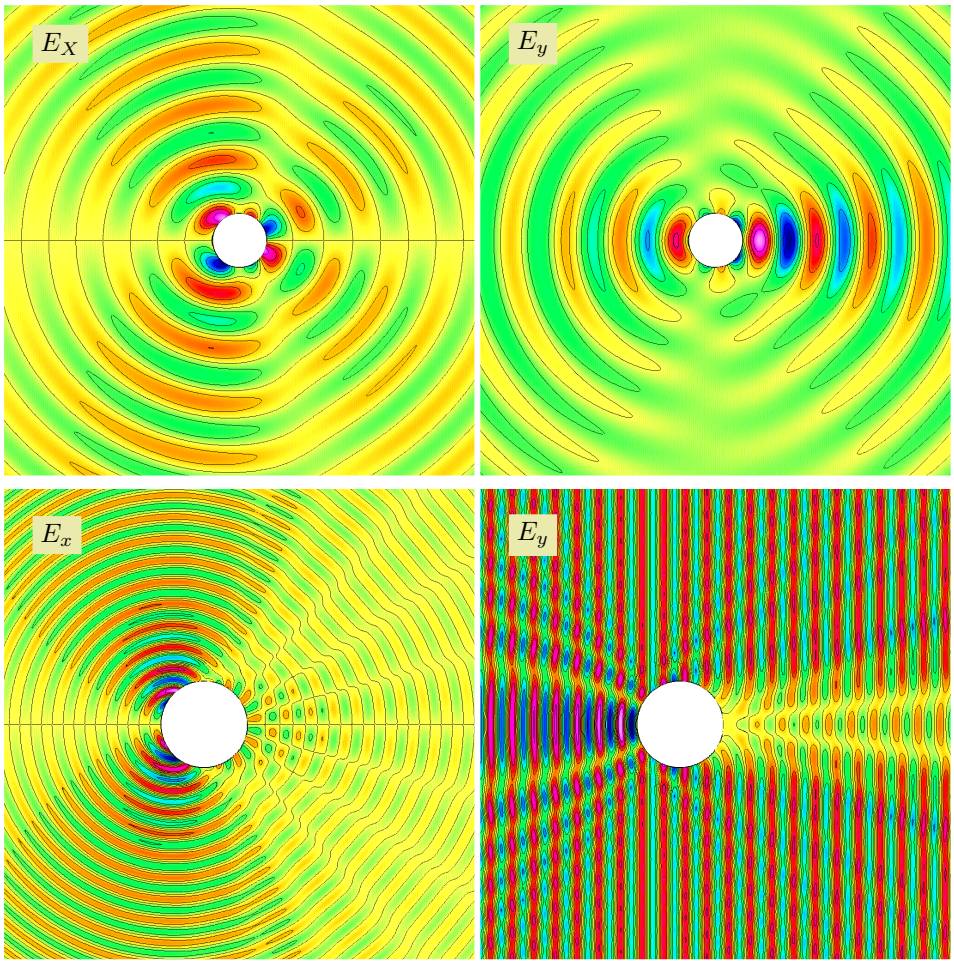

FIG. 8. *Scattering of a plane wave by a conducting cylinder of radius a. Top: scattered field E_x, E_y and H_z for $ka = \pi$ Bottom: total field E_x, E_y for $ka = 4\pi$.*

A PEC boundary condition is imposed on the cylinder. This boundary condition is adjusted to account for the removal of the incident field. Since $\mathbf{E} = \mathbf{E}^I + \mathbf{E}^S$ it follows that $\mathbf{n} \times \mathbf{E}^S = -\mathbf{n} \times \mathbf{E}^I$ on the PEC boundary. To avoid issues with far-field boundary conditions, the exact solution is imposed on the outer boundaries of the domain. The solution is integrated to time $t = 3$.

The coarse grid, $\mathcal{G}_1$, for the computational domain consists of a Cartesian grid for the square $[-2, 2]^2$ with 121×121 grid points and an annular grid centered at the origin with inner radius $a = \frac{1}{2}$, outer radius $\frac{3}{4}$ and with 161×9 grid points. Grids $\mathcal{G}_2$ and $\mathcal{G}_4$ are refined by factors of 2 and 4 in each direction compared to $\mathcal{G}_1$.

Table 4 presents the maximum errors and estimated convergence rates for the scattering by a incident wave with $k = 2\pi$ ($ka = \pi$). The results in the table indicate that the $\mathbf{E}$ and H_z fields are converging at rates close to 4. Figure 8 shows the solution for two different incident wave numbers, $ka = \pi$ and $ka = 4\pi$.

grid	$\|\mathrm{e}^{E_x}\|_\infty$	$\|\mathrm{e}^{E_y}\|_\infty$	$\|\mathrm{e}^{H_z}\|_\infty$	$\delta_{\mathbf{E}}$
$\mathcal{G}_1$	$4.0e{-4}$	$6.0e{-4}$	$1.3e{-4}$	$7.8e{-4}$
$\mathcal{G}_2$	$2.7e{-5}$	$4.1e{-5}$	$8.3e{-6}$	$6.3e{-5}$
$\mathcal{G}_4$	$1.8e{-6}$	$2.7e{-6}$	$5.2e{-7}$	$4.5e{-6}$
rate σ	3.93	3.91	4.01	3.74

TABLE 4

Maximum errors in the scattered field for the scattering of a plane wave by a two-dimensional PEC cylinder with $ka = \pi$. The maximum errors in E_x, E_y and H_z are given at $t = 3$ along with the estimated convergence rate. $\delta_{\mathbf{E}}$ is a non-dimensionalized divergence.

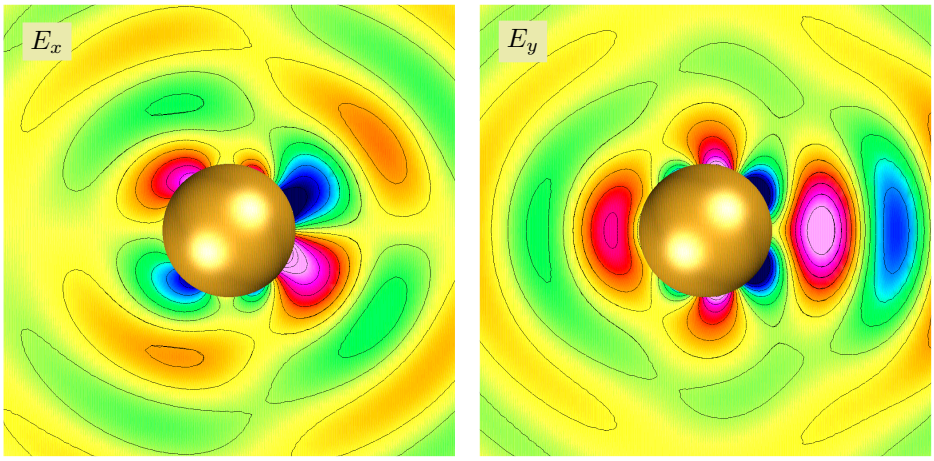

FIG. 9. *Scattering of a plane wave by a perfectly conducting sphere. The scattered fields for E_x and E_y are shown.*

10.4. Scattering by a PEC sphere. The three-dimensional computation of the scattering of a plane wave by a sphere of radius a is considered in this section. For an incident plane wave traveling in the x-direction, $\mathbf{E}^I = \left(e^{i(kx-\omega t)}, 0, 0\right)$, the total field in spherical polar coordinates (r, θ, ϕ) is given by the series expansion [39]

$$E_r = \frac{i\cos(\phi)}{(kr)^2}\sum_{n=1}^{\infty}(-i)^n(2n+1)\left[\psi_n(kr) - b_n\zeta_n^{(1)}(kr)\right]P_n^1(\cos(\theta))\; e^{-i\omega t}, \tag{10.3}$$

$$E_\theta = \frac{\cos(\phi)}{kr}\sum_{n=1}^{\infty}(-i)^n\frac{2n+1}{n(n+1)}\left[A_n\frac{P_n^1(\cos(\theta))}{\sin(\theta)} + iB_n\partial_\theta P_n^1(\cos(\theta))\right]\; e^{-i\omega t}, \tag{10.4}$$

$$E_\phi = -\frac{\sin(\phi)}{kr}\sum_{n=1}^{\infty}(-i)^n\frac{2n+1}{n(n+1)}\left[A_n\partial_\theta P_n^1(\cos(\theta)) + iB_n\frac{P_n^1(\cos(\theta))}{\sin(\theta)}\right]\; e^{-i\omega t}, \tag{10.5}$$

where P_n^1 are the Legendre polynomials and

$$A_n = \psi_n(kr) - a_n\zeta_n^{(1)}(kr) \quad , B_n = \psi_n'(kr) - b_n\zeta_n^{(1)'}(kr),$$
$$j_n(z) = \sqrt{\frac{\pi}{2z}}J_{n+1/2}(z), \quad h_n^{(1)}(z) = \sqrt{\frac{\pi}{2z}}H_{n+1/2}(z),$$
$$\psi(z) = zj_n(z), \quad \zeta_n^{(1)}(z) = zh_n^{(1)}(z), \quad a_n = \frac{\psi_n(ka)}{\zeta_n^{(1)}(ka)}, \quad b_n = \frac{\psi_n'(ka)}{\zeta_n^{(1)'}(ka)}.$$

The computed solution corresponds to the real part of equations (10.3-10.5).

As for the case of scattering of a plane wave by a cylinder, the known incident field can be subtracted out, leaving the solution to the scattered field, $\mathbf{E}^S$ to be determined. A PEC boundary condition is imposed on the surface of the sphere, taking into account the incident field that has been removed. The initial conditions are taken as the exact solution for the scattered field at times $t = -\Delta t$ and $t = 0$. The exact solution is imposed on the outer boundaries of the domain. The solution is integrated to time $t = 3$. The grids, $\mathcal{G}_1$, $\mathcal{G}_2$ and $\mathcal{G}_4$ used for the sphere in a box are the same as those described in section 10.1. Table 5 presents the maximum errors and estimated convergence rates. The computed values of $\mathbf{E}$ are converging at rates close to 4. Figure 9 shows the scattered field for an incident wave with $ka = \pi$.

10.5. Scattering of a plane wave by a dielectric cylinder. The two-dimensional computation of a plane wave hitting a dielectric (insulating) cylindrical disk possessing different material properties is used to test the accuracy of the material interface conditions presented in section 7. Consider a plane wave that is incident upon a

grid	$\|\mathrm{e}^{E_x}\|_\infty$	$\|\mathrm{e}^{E_y}\|_\infty$	$\|\mathrm{e}^{E_z}\|_\infty$	$\delta_{\mathbf{E}}$
$\mathcal{G}_1$	$1.3e{-}2$	$8.1e{-}3$	$6.7e{-}3$	$3.9e{-}3$
$\mathcal{G}_2$	$9.3e{-}4$	$5.8e{-}4$	$4.8e{-}4$	$4.2e{-}4$
$\mathcal{G}_4$	$6.2e{-}5$	$3.9e{-}5$	$3.2e{-}5$	$5.4e{-}5$
rate σ	3.86	3.86	3.85	3.09

TABLE 5

The maximum errors at $t = 3$ for the computation of a plane wave scattering from a perfectly conducting sphere.

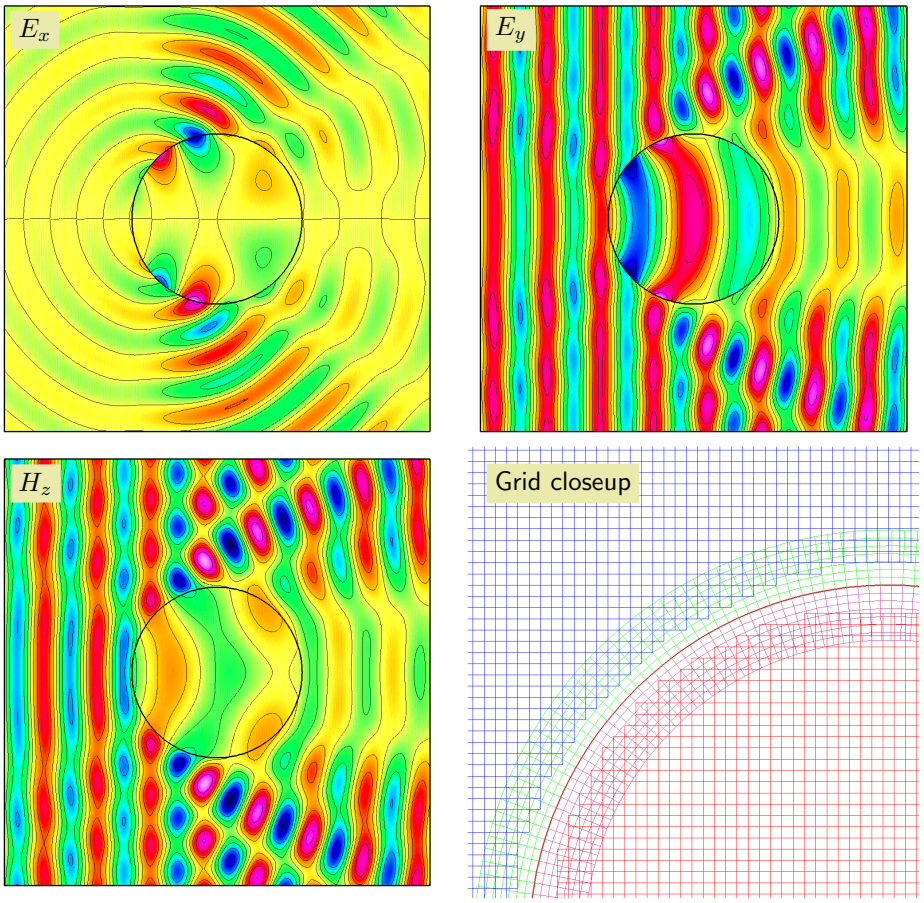

FIG. 10. *Scattering of a plane wave by a dielectric cylinder for $ka = 4\pi$. The field components E_x, E_y and H_z are shown for the solution computed on grid $\mathcal{G}_4$. A closeup of the grid $\mathcal{G}_2$ near the interface is shown.*

dielectric cylinder of radius a,

$$E_x^I = 0 \ , \quad E_y^I = \frac{\omega}{k} e^{i(kx-\omega t)} \ , \quad H_z^I = e^{i(kx-\omega t)} \ .$$

Let ϵ_i be the electric permittivity for the region interior to the cylinder, ϵ_o the electric permittivity for the region outside the cylinder and $m = \sqrt{\epsilon_i/\epsilon_o} = c_o/c_i$ the relative index of refraction for the dielectric. (The magnetic permeability μ is assumed to be the same in both materials). The solution for the magnetic field in terms of the incident, scattered field and dielectric field is of the form (see for example Balanis [2]

or van de Hulst [39]),

$$H_z^I = \sum_{n=-\infty}^{\infty} i^n J_n(kr) e^{in\theta}\ e^{-i\omega t}, \qquad \text{(incident plane wave)}, \tag{10.6}$$

$$H_z^S = \sum_{n=-\infty}^{\infty} i^n a_n H_n(kr) e^{in\theta}\ e^{-i\omega t}, \qquad \text{(scattered field for } r > a), \tag{10.7}$$

$$H_z^D = \sum_{n=-\infty}^{\infty} i^n b_n J_n(mkr) e^{in\theta}\ e^{-i\omega t}, \qquad \text{(dielectric field for } r < a), \tag{10.8}$$

where $H_n = H_n^{(2)} = J_n - iY_n$ is the Hankel function of the second kind. Imposing the interface jump conditions $[H_z] = 0$ and $[(H_z)_r/\epsilon] = 0$ at $r = a$ determines the coefficients a_n and b_n

$$\begin{aligned} a_n &= \big[J_n(ka)\ J_n'(mka) - mJ_n'(ka)\ J_n(mka)\big]/d_n, \\ b_n &= m\big[J_n(ka)\ H_n'(ka) - J_n'(ka)\ H_n(ka)\big]/d_n, \\ d_n &= mH_n'(ka)\ J_n(mka) - H_n(ka)\ J_n'(mka)\ . \end{aligned}$$

The computed solution corresponds to the real part of equations (10.6-10.8). A closeup of the grid used in this computation is shown in Figure 10. The coarse grid, $\mathcal{G}_1$, for this domain consists of four component grids. A Cartesian grid covers the domain $[-1,1]^2$ with 81×81 grid points. An annular grid of inner radius $a = \frac{1}{2}$, radial width .0875 and and 102×6 grid points covers the region immediately adjacent and exterior to the circle of radius $\frac{1}{2}$, centered at the origin. A second annular grid with the same radial width and grid spacing covers the region just inside the circle and a second Cartesian grid lies in the central region. The refined versions of the grids are $\mathcal{G}_2$ and $\mathcal{G}_4$. The width of the annular grids are decreased by the same factor of 2 as the grids are refined so that there remain 6 grid points in the radial direction. The initial conditions at $t = 0$ and $t = -\Delta t$ are taken as the exact solution. The boundary condition on the outer boundaries is also taken as the exact solution.

Table 6 shows convergence results for the scattering of a plane wave by the dielectric cylinder for an incident wave number of $ka = 4\pi$. The fourth-order accuracy of the method is evident. The solution is shown in Figure 10.

grid	$\|\mathrm{e}^{E_x}\|_\infty$	$\|\mathrm{e}^{E_y}\|_\infty$	$\|\mathrm{e}^{H_z}\|_\infty$	$\delta_{\mathbf{E}}$
$\mathcal{G}_1$	$1.4e{-1}$	$2.9e{-1}$	$3.0e{-1}$	$6.7e{-2}$
$\mathcal{G}_2$	$1.0e{-2}$	$2.1e{-2}$	$2.2e{-2}$	$4.5e{-3}$
$\mathcal{G}_4$	$6.8e{-4}$	$1.4e{-3}$	$1.4e{-3}$	$2.9e{-4}$
rate σ	3.86	3.87	3.88	3.92

TABLE 6

Maximum errors at $t = 1$ in computing the scattering of a plane wave by a dielectric cylinder. The incident wave number was $ka = 4\pi$,with $\epsilon = 1/4$ inside the cylinder and $\epsilon = 1$ in the region exterior to the cylinder.

10.6. Serial performance and memory usage. The performance of the **mx** solver on two problems, one two-dimensional and one three-dimensional, is given in table 7. The two-dimensional problem is for a circle in a channel grid, similar to the grids used in section 10.3. The three-dimensional problem considered the computation in the pill-pox geometry shown in Figure 11. The table indicates the amount of time that is spent in various parts of the code. In the two-dimensional case, close to 70% of the time is spent in the Fortran kernel that advances the solution on the interior points of the Cartesian grid. Advancing the solution on the curvilinear grids takes about 14% while applying the boundary conditions on all grids takes about 11%. These results show that the overall performance of the code is approaching that of a purely Cartesian grid solver, provided a sufficiently high percentage of the grids points are Cartesian grid points.

In three-dimensions, the advancement of the curvilinear grids takes the most time at about 48% with the Cartesian grids taking 28% and boundary conditions and interpolation taking a total of about 22%. In three-dimensions the cost of advancing the curvilinear grid with a fourth-order approximation is on the order of 10 times slower per grid point than for a Cartesian grid. As the grids are refined the percentage of Cartesian grid points will increase since the number of Cartesian grid points scales like N^3 while the number of curvilinear grids points grows like N^2 (assuming that the curvilinear boundary fitted grids retain a fixed number of grid points in the normal direction as the grids are refined). Thus for sufficiently fine grids in three-dimensions it can be expected that the time will be dominated by the work done on Cartesian grids.

	2D cylinder		3D pill-box	
	s/step	%	s/step	%
advance Cartesian grids	1.24	71.4	4.23	28.2
advance curvilinear grids	.242	14.0	7.18	47.8
boundary conditions	.184	10.6	2.23	14.8
interpolation	.008	0.46	1.01	6.8
other	.056	3.4	0.35	2.4
total	1.73	100	15.0	100

TABLE 7

CPU time (in seconds) per step for various parts of the code and their percentage of the total CPU time per step. Results for the two-dimensional cylinder in a channel problem (3.8 million grid points) are given in the two left columns. Results for the three-dimensional pill-box problem (10.2 million grid points) are given in the two right-most columns. Computations were performed on a desktop with a 2.2 GHz Zeon processor.

Table 8 gives the computer memory usage of the **mx** code for solving Maxwell's equations, to fourth-order accuracy, on the three-dimensional pill-box example of Figure 11. The table indicates the amount of memory required in MBytes for a double precision (64 bit) computation and the number of double precision floating point numbers required per grid point, denoted by reals/point. The number of reals/point for this computation was about 12.6. Only the **E** field was computed in this case. About 18% of the memory was dedicated to the storage of the overlapping grid (grid metrics, masks etc.). To put these numbers in context, note that if the Cartesian grids were treated as general curvilinear grids then the storage of the Jacobian matrix $\partial\mathbf{x}/\partial\mathbf{r}$ on the entire grid would itself require 9 reals/point. The **mx** solver is therefore seen to be quite memory efficient.

Memory Usage, Pill-box Problem			
	Mbytes	reals/pt	%
Overlapping grid	175.	2.3	17.8
Grid functions	779.	10.0	79.4
Other	26.	0.3	2.8
Total	980.	12.6	100.0

TABLE 8

Memory usage for the three-dimensional pill-box problem solved in double precision with the fourth-order accurate approximation. The grid for this problem contained about 10.2 *million grid points with about* 4.2e5 *interpolation points. The number of double precision floating point numbers required per grid point was about* 12.6 *(reals/pt). About* 17.8% *of the memory was dedicated to the storage of the overlapping grid (grid metrics, masks etc.).*

11. Conclusions. A scheme has been presented for the solution of the time-dependent Maxwell equations in complex geometries. The approach uses overlapping grids with a typical grid consisting of one or more background Cartesian grids overlapping body fitted curvilinear grids. Maxwell's equations are solved as a second-order vector wave equation. A three-level time stepping scheme is used that can be used to generate methods of order $2, 4, 6, \ldots$. High-order accurate symmetric finite difference approximations to the generalized Laplace operator have been developed. These

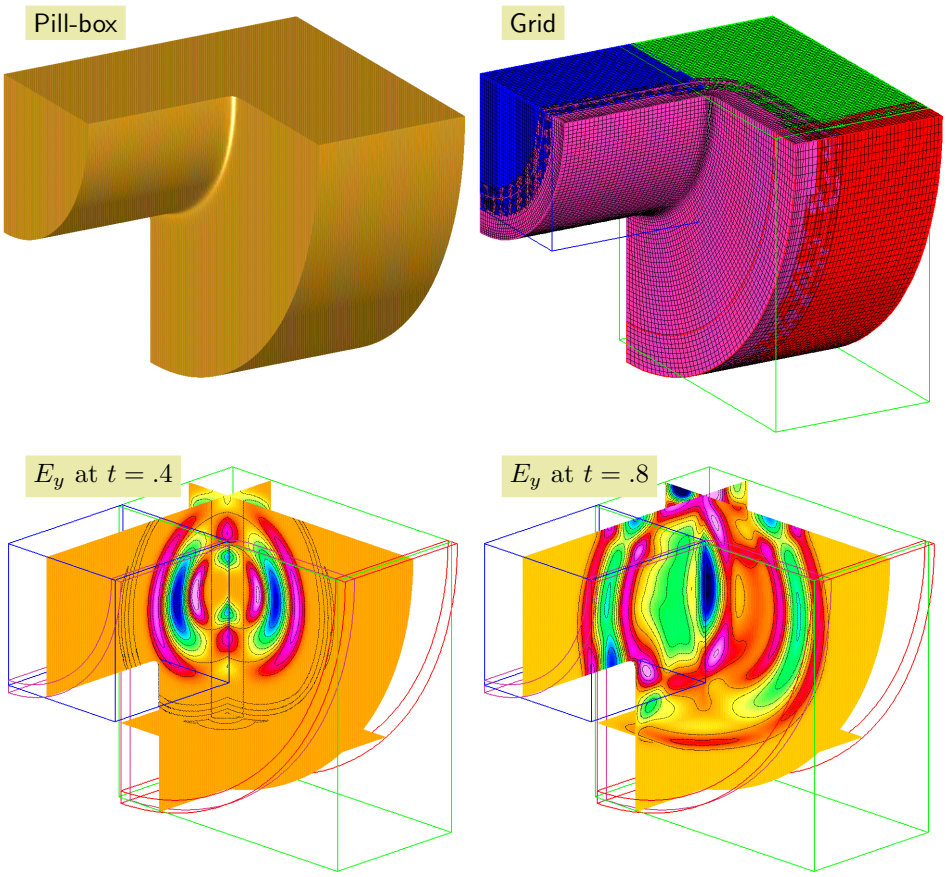

FIG. 11. *Propagation of a pulse in a pill-box cavity. Top left: the pill-box geometry. Top-right: the overlapping grid for the geometry (coarse grid version). Bottom: the electric field component E_y at two times. Contours of the field are plotted on planes that cut through the computational domain. The block-boundaries of the the grids are shown for reference.*

approximations are symmetric on arbitrary logically rectangular curvilinear grids. Implementations of these operators in two- and three-dimensions for orders 2, 4, 6 and 8 were shown to give energy preserving results when solving Maxwell's equations on a square and a box with randomly perturbed grid points. High-order accurate centered boundary conditions for perfect electrical conductor (PEC) boundaries have been devised. High-order accurate centered boundary conditions were also developed for material interfaces that separate regions with constant values of the material properties. The interfaces were represented with overlapping grids, using boundary fitted grids on each side of the interface. These centered boundary conditions are based on compatibility conditions derived from the governing equations. The stability and accuracy of the fourth-order accurate PEC approximations were analyzed for a model problem on a periodic strip. The stability of the material interface conditions were analyzed for a one-dimensional model problem for a second- and fourth-order approximation.

The approach has been implemented for computations on distributed memory multi-processor machines. The arrays holding the solution variables and grid metrics etc. on each component grid are distributed across one or more processors. An efficient parallel interpolation scheme has been developed for communicating the interpolation information where component grids overlap. Results from parallel computations show that the algorithm scales well.

Numerical results for a number of two- and three-dimensional problems were used to verify the accuracy of the fourth-order accurate version of the method. In all cases the accuracy, in the maximum norm, was shown to be close to four. The method

of analytic solutions was used to generate *exact* solutions to the forced equations and verify the convergence rates. The eigenmodes of a three-dimensional cylindrical cavity were computed and compared to the known eigenmodes. The scattering of a plane wave by a two-dimensional cylinder and a three-dimensional sphere were computed and compared to the exact series solutions. The material interface boundary conditions were tested in two-dimensions for the scattering of a plane wave by a dielectric cylinder, and compared to the exact solution. Statistics presented from some representative computations showed that the method is very efficient in both speed and memory, especially when the overlapping grid for the domain consists mainly of Cartesian grid points. In that case the performance of the method can approach that of a Cartesian grid solver.

The **mx** Maxwell solver has been implemented using the Overture framework. Overture has support for adaptive mesh refinement, moving grids and fast multigrid solvers for elliptic equations[20, 19]. These capabilities of Overture may be useful for future extensions of the the Maxwell solver. Far-field boundary conditions for boundaries of the computational domain that have been artificially truncated are an important consideration. The treatment of these far-field boundary conditions in conjunction with the present approach is left to a future publication.

Acknowledgments: The author would like to thank Professor Heinz-Otto Kreiss for many useful discussions.

REFERENCES

[1] L. Anné, P. Joly, and Q. H. Tran, *Construction and analysis of higher order finite difference schemes for the 1d wave equation*, Computational Geosciences, 4 (2000), pp. 207–249.
[2] C. A. Balanis, *Advanced Engineering Electromagnetics*, John Wiley & Sons, 1989.
[3] M. Born and E. Wolf, *Principles of Optics*, Cambridge University Press, Cambridge, 2002.
[4] G. Browning, *A comparison of three numerical methods for solving differential equations on the sphere*, Monthly Weather Review, 117 (1989), pp. 1058–1075.
[5] G. Chesshire and W. Henshaw, *Composite overlapping meshes for the solution of partial differential equations*, J. Comp. Phys., 90 (1990), pp. 1–64.
[6] G. C. Cohen, *Higher-Order Numerical Methods for Transient Wave Equations*, Springer, New York, 2002.
[7] M. Dablain, *The application of high order differencing for the scalar wave equation*, Geophysics, 51 (1986), pp. 54–66.
[8] S. Dey and R. Mittra, *A locally conformal finite-difference time-domain (FDTD) algorithm for modeling three-dimensional perfectly conducting objects*, IEEE Microwave and Guided Wave Letters, 7 (1997), pp. 273–275.
[9] A. Ditkowksi, K. Dridi, and J. Hesthaven, *Convergent Cartesian grid methods for Maxwell's equations in complex geometries*, Journal of Computational Physics, 170 (2001), pp. 39–80.
[10] T. A. Driscoll and B. Fornberg, *A block pseudospectral method for Maxwell's equations I: One-dimensional case*, Journal of Computational Physics, 140 (1998), pp. 47–65.
[11] ———, *Block pseudospectral methods for Maxwell's equations II: Two-dimensional, discontinuous coefficients case*, SIAM J. Sci. Comput., 21 (1999), pp. 1146–1167.
[12] B. Fornberg, *A Practical Guide to Pseudospectral Methods*, Cambridge University Press, 1996.
[13] S. D. Gedney, F. S. Lansing, and D. L. Rascoe, *Full wave analysis of microwave monolithic circuit devices using a generalized Yee-algorithm based on an unstructured grid*, IEEE Transactions on Microwave Theory and techniques, 44 (1996), pp. 1393–1400.
[14] B. Gustafsson, H.-O. Kreiss, and J. Oliger, *Time Dependent Problems and Difference Methods*, John Wiley and Sons Inc., 1995.
[15] B. Gustafsson and E. MossBerg, *Time compact high order difference methods for wave propagation problems*, SIAM J. Sci. Comput., 26 (2004), pp. 259–271.
[16] W. Henshaw, *A fourth-order accurate method for the incompressible Navier-Stokes equations on overlapping grids*, J. Comp. Phys., 113 (1994), pp. 13–25.
[17] ———, *Ogen: An overlapping grid generator for Overture*, Research Report UCRL-MA-132237, Lawrence Livermore National Laboratory, 1998.
[18] W. Henshaw, H.-O. Kreiss, and L. Reyna, *A fourth-order accurate difference approximation for the incompressible Navier-Stokes equations*, Comput. Fluids, 23 (1994), pp. 575–593.
[19] W. D. Henshaw, *On multigrid for overlapping grids*, SIAM Journal of Scientific Computing, 26 (2005), pp. 1547–1572.
[20] W. D. Henshaw and D. W. Schwendeman, *An adaptive numerical scheme for high-speed reactive flow on overlapping grids*, J. Comp. Phys., 191 (2003), pp. 420–447.
[21] J. Hesthaven and T. Warburton, *Nodal high-order methods on unstructured grids, I. time-*

domain solution of Maxwell's equations, J. Comp. Physics, 181 (2002), pp. 186–221.

[22] R. Holland, *Finite difference solution of Maxwell's equations in generalized nonorthogonal coordinates*, IEEE Transactions on Nuclear Science, 30 (1983), pp. 4589–4591.

[23] J. Jin, *The Finite Element Method in Electromagnetics*, John Wiley and Sons, New York, 1993.

[24] H. Jurgens and D. Zingg, *Numerical solution of the time-domain Maxwell equations using high-accuracy finite-difference methods*, SIAM J. Sci. Comput., 22 (2000), pp. 1675–1696.

[25] H.-O. Kreiss, N. A. Petersson, and J. Ystrom, *Difference approximations for the second order wave equation*, SIAM J. Numer. Anal., 40 (2002), pp. 1940–1967.

[26] J. Lambert, *Computational Methods in Ordinary Differential Equations*, Cambridge University Press, New York, 1973.

[27] J. Lee, R. Palendech, and R. Mittra, *Modeling three-dimensional discontinuities in waveguides using nonorthogonal FDTD algorithm*, IEEE Trans. Microwave Theory and Techniques, 40 (1992), pp. 346–352.

[28] N. K. Madsen, *Divergence preserving discrete surface integral method for Maxwell's curl equations using non-orthognal unstructured grids*, J. Comp. Phys., 119 (1995), pp. 34–45.

[29] J. Nédélec, *Mixed finite elements in R^3*, Numer. Math., 35 (1980), pp. 315–341.

[30] D. Quinlan, *A++/P++ class libraries*, Research Report LA-UR-95-3273, Los Alamos National Laboratory, 1995.

[31] L. G. M. Reyna, *Part III. On Composite Meshes*, PhD thesis, Dept. of Applied Mathematics, California Institute of Technology, 1982.

[32] P. Roache, *Code verification by the method of manufactured solutions*, ASME J. of Fluids Engineering, 124 (2002), pp. 4–10.

[33] G. Rodrigue and D. White, *A vector finite element time-domian method for solving Maxwell's equations on unstructured hexahedral grids*, SIAM J. Sci. Comput., 23 (2001), pp. 683–706.

[34] T. Rylander and A. Bondeson, *Application of stable FEM-FDTD hybrid to scattering problems*, IEEE Transactions on Antennas and Propogation, 50 (2002), pp. 141–144.

[35] G. R. Shubin and J. B. Bell, *A modified equation approach to constructing fourth order schemes for acoustic wave propagation*, SIAM J. Sci. Stat. Comput., 8 (1987), pp. 135–151.

[36] A. Sussman, G. Agrawal, and J. Saltz, *A manual for the Multiblock PARTI runtime primitives, revision 4.1*, Technical Report CS-TR-3070.1, University of Maryland, Department of Computer Science, 1993.

[37] A. Taflove and S. C. Hagness, *Computational Electrodynamics: The Finite-Difference Time-Domain Method*, Artech House, 2000.

[38] O. team, *Overture home page*, Tech. Rep. http://www.llnl.gov/CASC/Overture.html, Lawrence Livermore National Laboratory, 2002.

[39] H. van de Hulst, *Light Scattering by Small Particles*, Dover Publications, Inc., 1957.

[40] B. Yang, D. Gottlieb, and J. Hesthaven, *Spectral simulations of electromagnetic wave scattering*, J. Comp. Physics, 134 (1997), pp. 216–230.

[41] K. Yee, *Numerical solution of initial boundary value problems involving Maxwell's equations in isotropic media*, IEEE Transactions on Antennas and Propogation, 14 (1966), pp. 302–307.

[42] K. S. Yee, J. S. Chen, and A. H. Chang, *Conformal finite-difference time-domain (FDTD) with overlapping grids*, IEEE Transactions on Antennas and Propogation, 40 (1992), pp. 1068–1075.